

Fast and accurate predictions of the nonlinear matter power spectrum for general models of Dark Energy and Modified Gravity

B. Bose^{1,2*}, M. Tsedrik¹, J. Kennedy^{2,3}, L. Lombriser², A. Pourtsidou^{1,4}, A. Taylor^{1,4}.

¹*Institute for Astronomy, University of Edinburgh, Royal Observatory, Blackford Hill, Edinburgh, EH9 3HJ, U.K.*

²*Département de Physique Théorique, Université de Genève, 24 quai Ernest Ansermet, 1211 Genève 4, Switzerland.*

³*The Global Academy of Agriculture and Food Systems, University of Edinburgh, Easter Bush Campus, Charnock Bradley Building, EH25 9RG.*

⁴*Higgs Centre for Theoretical Physics, School of Physics and Astronomy, The University of Edinburgh, Edinburgh EH9 3FD, UK.*

arXiv:2210.01094v1 [astro-ph.CO] 3 Oct 2022

Accepted XXX. Received YYY; in original form ZZZ

ABSTRACT

We embed linear and nonlinear parametrisations of beyond standard cosmological physics in the halo model reaction framework, providing a model-independent prescription for the nonlinear matter power spectrum. As an application, we focus on Horndeski theories, using the Effective Field Theory of Dark Energy (EFTofDE) to parameterise linear and quasi-nonlinear perturbations. In the nonlinear regime we investigate both a nonlinear parameterised-post Friedmann (nPPF) approach as well as a physically motivated and approximate phenomenological model based on the error function (Erf). We compare the parameterised approaches' predictions of the nonlinear matter power spectrum to the exact solutions in two well studied modified gravity models, finding sub-percent agreement using the Erf model at $z \leq 1$ and $k \leq 5 \text{ h/Mpc}$. This suggests only an additional 3 free constants, above the background and linear theory parameters, are sufficient to model nonlinear, non-standard cosmology in the matter power spectrum at scales down to $k \leq 3 \text{ h/Mpc}$ within 2% accuracy. We implement the parametrisations into ver.2.0 of the ReACT code: [ACTio et ReACTio](#).

Key words: cosmology: theory – large-scale structure of the Universe – methods: analytical – methods: numerical

1 INTRODUCTION

Fundamental models of nature generally begin with an action, which when combined with the principle of least action, gives us the temporal and spatial dynamics of the system. For the physical system that is our Universe (U), the action is widely accepted to be the action associated with general relativity (GR), the Einstein-Hilbert (EH) action, together with a matter contribution and cosmological constant

$$S_U = S_{\text{EH}} + S_M = \int d^4x \sqrt{-g} \left[\frac{R}{2\kappa^2} - \frac{\Lambda}{\kappa^2} \right] + S_M, \quad (1)$$

where $\kappa^2 = 8\pi G_N$, G_N being Newton's gravitational constant and R is the 4-dimensional Ricci scalar that gauges the curvature of space-time. S_M is the action of the matter content of the Universe, usually approximated by a perfect, pressureless fluid, but in general will contain all Standard Model fields. Λ is the (cosmological) constant that can appear naturally in a 4-dimensional action without violating preferred symmetries (see, for example, [Fernandes et al. 2022](#)). This constant is measured to be non-zero by a suite of cosmological probes such as the cosmic microwave background (CMB) radiation ([Aghanim et al. 2020](#)), type 1a supernovae ([Riess et al. 1998](#); [Perlmutter et al. 1999](#)), and optical galaxy surveys (see, for example,

[Alam et al. 2021](#)). This has led to the standard model of cosmology, Λ CDM, where CDM stands for cold dark matter¹.

Consistently, we would expect a non-zero cosmological constant from quantum field theory (QFT) predictions, as all vacuum states of standard model particle fields will contribute an energy density, ρ_{vac} , to the Universe that appears as a constant in the model's action. Unfortunately, this results in one of the biggest problems in physics (see [Martin 2012](#), for a review). The first aspect of the problem is that our naïve (QFT) predictions for the energy density of Λ is at least 60 orders of magnitude larger than the (cosmological) measured value². We can still make a (fine) tuning of the 'bare' constant Λ_{bare} in the potentials of these fields to cancel the other vacuum energy contributions to yield the observed value for Λ .

One might be fine with this, after all QFTs are used to removing divergences through renormalisation techniques. The real problem is that we need to repeatedly fine tune every time a new energy scale or particle field is considered which changes ρ_{vac} (this can also happen through phase transitions) (see [Padilla 2015](#), for an overview). In other words, the value of Λ , which is a low energy physics parameter, is incredibly sensitive to the high energy physics, which is not technically natural and in apparent opposition to our wide spread employment of effective field theories. These two aspects of

¹ CDM is the primary matter component in this model, outweighing baryonic matter five fold according to cosmological and astrophysical measurements such as the CMB.

² This depends on the energy scales we are considering in the QFT calculation.

* E-mail:ben.bose@ed.ac.uk

the problem are often referred to collectively as the ‘cosmological constant problem’. We refer the interested reader to the seminal paper by Weinberg (1989) for a review and the famous no-go theorem which implicitly delineates possible solutions to the problem.

Prospective solutions to these problems include gravitationally screening the vacuum energy from our observations by using a scalar field (for example, Charmousis et al. 2012; Appleby & Linder 2020; Sobral Blanco & Lombriser 2020; Khan & Taylor 2022) or using extra spacetime dimensions (for example, Burgess 2004). These solutions would of course also need to produce a small residual energy that can be used to explain our cosmological measurements, in particular those associated with an accelerated spatial expansion. This distinct issue can be called the ‘dark energy problem’, which may be explained through a variation in the fundamental constants of nature such as Newton’s gravitational constant, or having the acceleration driven by a scalar field (see Thomas et al. 2022, for a general parameterisation of such options).

The dark energy and cosmological constant problems motivate a minimal extension of Equation 1 to include a single extra scalar degree of freedom, ϕ , which is both physically and theoretically acceptable, i.e., not allowing for negative energies for example, and can encapsulate one or more cosmological constant problem solutions. Such an extension is found in the well studied Horndeski (H) scalar-tensor theory (Horndeski 1974). This is the most general, Lorentz-covariant scalar-tensor theory in 4 spacetime dimensions that yields second-order equations of motion, a basic condition for the physical viability of the theory, i.e., it is ghost-free. A universe described by Horndeski gravity is given as

$$S_U = S_H + S_M = \int d^4x \sqrt{-g} \left[G_2(\phi, X) - G_3(\phi, X) \square \phi + G_4(\phi, X) R \right. \\ \left. + G_{4,X}(\phi, X) [(\square \phi)^2 - (\nabla_\mu \nabla_\nu \phi)^2] \right. \\ \left. + G_5(\phi, X) G_{\mu\nu} \nabla^\mu \nabla^\nu \phi \right. \\ \left. - \frac{1}{6} G_{5,X}(\phi, X) [(\square \phi)^3 - 3 \square \phi (\nabla_\mu \nabla_\nu \phi)^2 + 2 (\nabla_\mu \nabla_\nu \phi)^3] \right] \\ + S_M, \quad (2)$$

where each $G_i(\phi, X)$, $i = 2, 3, 4, 5$ is a free function of the scalar field ϕ and its canonical kinetic term $X = -(\partial \phi)^2/2$, and $G_{i,X}(\phi, X) = \partial G_i / \partial X$.

This opens up a very large theory space which needs to be trimmed down with observational data. We have very strong data constraints at small spatial scales, i.e., within the Solar System and at astrophysical scales (Will 1993; Will 2014), showing gravity is highly consistent with GR in this regime. We also have high quality observational data from cosmology, primarily from the CMB which is associated with early cosmological times. This allows new theoretical models most phenomenological freedom at large temporal and spatial scales as they must recover CMB and solar system observations. The small spatial scale constraints can be evaded using so called *screening mechanisms* (see Koyama 2018; Burrage & Sakstein 2018, for reviews) that force predictions of modified gravity models back to those of GR locally, while early time measurements like the CMB can easily be recovered through appropriate time evolution of ϕ .

An obvious late time cosmological data set directly related to gravity is the large scale structure of the Universe (LSS). A key summary statistic of this is the two point correlation function or *power spectrum* (in Fourier space) of the cosmological matter field. A prime science goal then becomes the production of accurate predictions of the matter power spectrum in general theories beyond- Λ CDM. For the Horndeski class of models, this is a nontrivial task as there are

an additional four free functions of space and time to contend with, beyond the matter content and metric freedoms. Of course, one can always choose particular forms for the $G_i(\phi, X)$ and then produce predictions for the 2-point correlations of matter. This approach allows one to fully specify how matter should cluster at all physical scales, and there are many tools and models that do just that to varying degrees of accuracy (Schmidt et al. 2010; Lombriser 2014; Arnold et al. 2021; Cataneo et al. 2019; Bose et al. 2020; Hernández-Aguayo et al. 2022; Puchwein et al. 2013; Brax & Valageas 2013, 2014; Joudaki et al. 2022; Winther et al. 2017).

If on the other hand we choose not to specify a particular model, we are required to parameterise both the linear and nonlinear scales i.e., the large and small physical scales of LSS respectively. At linear scales and for the Horndeski class of models, we can opt to perform a Taylor expansion of the G_i functions and truncate at some order. Linear theory can then be characterised by a small number of free functions of time but with no unique specification in the nonlinear regime. This describes the approach of the Effective Field Theory of Dark Energy (EFTofDE) by Gubitosi et al. (2013); Bloomfield et al. (2013) (also see Frusciante & Peron 2020, for a review). Note that if we wish to be even more general than Horndeski we can directly parameterise the linear relation between matter and the gravitational potential.

On nonlinear scales, a parameterisation framework one can consider is the nonlinear parameterised post-Friedmannian (nPPF), which captures modified gravity or dark energy effects (Lombriser 2016). Both linear and nonlinear parameterisations then need to be consistently embedded in some more comprehensive predictive framework in order to be able to confront theory with LSS observations.

For past galaxy surveys the precision of the data did not call for high accuracy in the power spectrum modelling, (as argued in Spurio Mancini et al. 2019; Traykova et al. 2019). This changes with the next generation of surveys (Stage-IV) such as Euclid³ (Laureijs et al. 2011) and the Vera C. Rubin Observatory’s Legacy Survey of Space and Time (LSST)⁴ (Ivezic et al. 2019). These surveys will provide a significant reduction in statistical errors, errors which will be lowest in the nonlinear regime. With such precision, we have the opportunity to greatly constrain deviations to Λ CDM, including the well defined model space within Equation 2. This is contingent on whether or not we can accurately and efficiently map these deviations to the matter power spectrum. Typically, to remain unbiased in our constraints on Nature, $\mathcal{O}(1)\%$ is quoted as being the target accuracy for theoretical predictions (see Blanchard et al. 2020a, for example). But this is not sufficient. We also require this map to be computationally efficient enough to perform data analyses. Without accuracy, we forfeit trust in our constraints. Without conciseness and efficiency we face major computational issues.

This paper provides a balance that satisfies these criteria. We mainly focus on the Horndeski class of models, embedding the EFTofDE and nPPF approaches into the halo model reaction framework (Cataneo et al. 2019; Giblin et al. 2019; Cataneo et al. 2020; Bose et al. 2019, 2020; Carrilho et al. 2022), which is able to predict the nonlinear power spectrum for specified theories beyond- Λ CDM at $\mathcal{O}(1)\%$ -level accuracy. We also present a completely model independent parametrisation of beyond- Λ CDM physics at nonlinear scales, which can be combined with similar parametrisations for the Universe’s background expansion history and linear structure forma-

³ <http://euclid-ec.org>

⁴ <https://www.lsst.org/>

tion, giving a parametrisation for general deviations to Λ CDM. Thus, this work promotes the halo model reaction framework to being able to perform model independent predictions, a key step in the search for a more fundamental description of Nature in the cosmological, low energy regime.

This paper is organised as follows: in section 2 we begin at the observational end and look how to model the (halo model) *reaction*. In section 3 we jump to the theoretical end, and look how we can connect the ingredients of the reaction to an *action* of Nature, together with any additional degrees of freedom characterising nonlinear physics. In section 4 we give an overview of the mapping between the reaction and the parameterisations of gravity and dark energy, along with some key simplifying approximations one can consider. We also perform tests and provide motivations for these approximations. Then, in section 5 we test the proposed parameterisations by comparing to exact predictions in two representative non-standard models of gravity. In section 6 we summarise our results and conclude. In the appendices we provide full expressions for the linear and nonlinear parametrisations as well as illustrative examples and comparisons within specific non-standard models of gravity.

2 HALO MODEL REACTION

The leading order moment of the cosmological matter distribution is the *nonlinear matter power spectrum*, $P_{\text{NL}}(k, z)$. This Fourier space quantity captures most of the matter clustering information at all scales (see Bernardeau et al. 2002, for a review). Following the halo model (see Cooray & Sheth 2002, for a review) based approach of Cataneo et al. (2019), in a target theory of cosmology and gravity this quantity can be modelled as

$$P_{\text{NL}}(k, z) = \mathcal{R}(k, z) P_{\text{NL}}^{\text{pseudo}}(k, z), \quad (3)$$

where $P_{\text{NL}}^{\text{pseudo}}(k, z)$ is called the pseudo power spectrum. This is defined as the power spectrum of a Λ CDM universe but whose initial conditions have been set so as to match the target, beyond- Λ CDM, theory's linear total matter power spectrum $P_L(k, z)$ at some target redshift, z . The reason for making such a definition is that it guarantees the halo mass functions in the target and pseudo universes are similar since they will have the same linear clustering by definition. This results in a smoother transition between the clustering statistics in the inter- and intra-halo regimes. This quantity can be modelled in a number of ways, for example by using existing halo model based fitting functions such as HMCode (Mead et al. 2015, 2016; Mead et al. 2021) or for target theories that only predict a redshift dependent, but scale independent rescaling of the linear spectrum, Λ CDM-based emulators such as EuclidEmulator2 (Euclid Collaboration et al. 2020) or bacco (Angulo et al. 2021) can be used by tuning the spectrum amplitude parameter to match the modified cosmology's linear spectrum.

The function $\mathcal{R}(k, z)$ represents all the corrections to the pseudo spectrum coming from nonlinear beyond- Λ CDM physics. Following Cataneo et al. (2020); Bose et al. (2021) we can write this as

$$\mathcal{R}(k) = \frac{(1 - f_\nu)^2 P_{\text{hm}}^{(\text{cb})}(k) + 2f_\nu(1 - f_\nu) P_{\text{hm}}^{(\text{cb}\nu)}(k) + f_\nu^2 P_L^{(\nu)}(k)}{P_{\text{hm}}^{\text{pseudo}}(k, z)}, \quad (4)$$

with the subscript 'hm' standing for halo model, $(\text{m}) \equiv (\text{cb} + \nu)$, cb for CDM and baryons, ν for massive neutrinos and $f_\nu = \Omega_{\nu,0}/\Omega_{m,0}$ being the massive neutrino energy density fraction at $z = 0$. The effects of massive neutrinos are included linearly through the weighted

sum of the nonlinear cb halo model and linear massive neutrino spectra following the findings of Agarwal & Feldman (2011). We note that we do not consider massive neutrino effects in this work, but have included them in the expressions to highlight the generality of this approach (see Bose et al. 2021, for a study with massive neutrinos).

The individual components are given by

$$P_{\text{hm}}^{(\text{cb}\nu)}(k) \approx \sqrt{P_{\text{hm}}^{(\text{cb})}(k) P_L^{(\nu)}(k)}, \quad (5)$$

$$P_{\text{hm}}^{(\text{cb})}(k) = \left[(1 - \mathcal{E}) e^{-k/k_\star} + \mathcal{E} \right] P_L^{(\text{cb})}(k) + P_{1\text{h}}^{(\text{cb})}(k), \quad (6)$$

$$P_{\text{hm}}^{\text{pseudo}}(k, z) = P_L(k, z) + P_{1\text{h}}^{\text{pseudo}}(k, z), \quad (7)$$

where the parameters are given by

$$\mathcal{E}(z) = \lim_{k \rightarrow 0} \frac{(1 - f_\nu)^2 P_{1\text{h}}^{(\text{cb})}(k, z)}{P_{1\text{h}}^{\text{pseudo}}(k, z)}, \quad (8)$$

$$k_\star(z) = -\bar{k} \left(\ln \left[\frac{T_1(\bar{k}, z) \pm T_2(\bar{k}, z)}{(1 - f_\nu)^2 P_L^{(\text{cb})}(\bar{k}, z)(1 - \mathcal{E}(z))} \right] \right)^{-1}. \quad (9)$$

We take the '+' root if $\mathcal{E} > 1$, otherwise we take the '-' root. The T_i terms are given by

$$T_1(k, z) = f_\nu^2 P_L^{(\nu)}(k, z) + P_{\text{hm}}^{\text{pseudo}}(k, z) \mathcal{R}_{\text{SPT}}(k, z) - (1 - f_\nu)^2 [\mathcal{E}(z) P_L^{(\text{cb})}(k, z) + P_{1\text{h}}^{(\text{cb})}(k, z)], \quad (10)$$

$$T_2(k, z) = 2\sqrt{f_\nu^2 P_{\text{hm}}^{\text{pseudo}}(k, z) P_L^{(\nu)}(k, z) \mathcal{R}_{\text{SPT}}(k, z)}, \quad (11)$$

where $\mathcal{R}_{\text{SPT}}(k, z)$ is the 1-loop standard perturbation theory (SPT) (Bernardeau et al. 2002) prediction for the reaction given by Equation 4-7 but with the replacements $P_L(k, z) \rightarrow P_{1\text{-loop}}(k, z)$ and $P_L(k, z)^{(\text{cb})} \rightarrow P_{1\text{-loop}}(k, z)^{(\text{cb})}$ and $\mathcal{E} = 1$. As in Cataneo et al. (2019) the default scale where we calculate k_\star is set to $\bar{k} = 0.06 h \text{ Mpc}^{-1}$.

We see that Equation 4 depends on three general predictions for beyond- Λ CDM theories: the 2-halo term which we have approximated by the linear power spectrum P_L , the quasi-nonlinear power spectrum given by the 1-loop perturbation theory power spectrum $P_{1\text{-loop}}$, and the highly nonlinear power spectrum given by the 1-halo term $P_{1\text{h}}$. The computation of these quantities requires the specification of the matter density fluctuations at different physical scales. The first two regimes (linear and quasi-nonlinear) are perturbatively derived up to 3rd order in the linear density fluctuation δ_L , while the fully nonlinear quantity, δ_{NL} , can be obtained using the assumptions of spherical collapse (Cooray & Sheth 2002). Both these routes require us to solve differential equations representing energy and momentum conservation on a cosmological background. Our Universe's spacetime metric is well described by the Friedmann-Lemaître-Robertson-Walker (FLRW) metric, whose background expansion is described by the Hubble parameter $H(a) \equiv \dot{a}/a$, where a is the scale factor and an over-dot represents a derivative with respect to the metric time t .

Further, the conservation equations rely on the relation between the gravitational potential and the matter density fluctuation: the *Poisson equation*. In particular, we consider the Poisson equation in the perturbative limit, only valid up to quasi-nonlinear scales, as well

as the fully nonlinear expression, valid at all scales

$$-\left(\frac{k}{aH(a)}\right)^2 \Phi_{\text{QNL}}(\mathbf{k}, a) = \frac{3\Omega_m(a)}{2} \mu(k, a) \delta_{\text{QNL}}(\mathbf{k}, a) + S(\mathbf{k}, a), \quad (12)$$

$$-\left(\frac{k}{aH(a)}\right)^2 \Phi_{\text{NL}}(\mathbf{k}, a) = \frac{3\Omega_m(a)}{2} [1 + \mathcal{F}(k, a)] \delta_{\text{NL}}(\mathbf{k}, a), \quad (13)$$

where $\Omega_m(a) = \Omega_{m,0} H_0^2 / (H(a)^2 a^3)$, $\Omega_{m,0}$ being the total matter fraction today. Φ is the gravitational potential in the time-time component of the perturbed FLRW metric. This can be identified with the Newtonian gravitational potential in the non-relativistic limit, valid for the curvatures and velocities we consider. The subscripts QNL and NL denote ‘quasi-nonlinear’ and ‘nonlinear’ respectively.

The additional functions in [Equation 12](#) and [Equation 13](#) are as follows: $\mu(k, a)$ characterises the linear modification to GR, $\mathcal{F}(k, a)$ is the nonlinear modification and $S(\mathbf{k}, a)$ is a source term capturing modifications at 2nd and 3rd order in the linear matter density perturbations. The source term is given by ([Bose & Koyama 2016](#))

$$S(\mathbf{k}, a) = \int \frac{d^3 \mathbf{k}_1 d^3 \mathbf{k}_2}{(2\pi)^3} \delta_D(\mathbf{k} - \mathbf{k}_{12}) \gamma_2(\mathbf{k}_1, \mathbf{k}_2, a) \delta(\mathbf{k}_1) \delta(\mathbf{k}_2) + \int \frac{d^3 \mathbf{k}_1 d^3 \mathbf{k}_2 d^3 \mathbf{k}_3}{(2\pi)^6} \delta_D(\mathbf{k} - \mathbf{k}_{123}) \gamma_3(\mathbf{k}_1, \mathbf{k}_2, \mathbf{k}_3, a) \times \delta(\mathbf{k}_1) \delta(\mathbf{k}_2) \delta(\mathbf{k}_3), \quad (14)$$

introducing two additional functions γ_2 & γ_3 characterising quasi-nonlinear modifications to the Poisson equation (see [Bose & Koyama 2016](#), for explicit expressions for these in the Horndeski class of models).

In total, the halo model reaction, and so the nonlinear power spectrum, requires specification of four functions of space and time - one for the background $H(a)$, one for the linear regime $\mu(k, a)$, two for the quasi-nonlinear regime $\gamma_2(\mathbf{k}_1, \mathbf{k}_2, a)$ & $\gamma_3(\mathbf{k}_1, \mathbf{k}_2, \mathbf{k}_3, a)$ and finally one for the fully nonlinear regime $\mathcal{F}(k, a)$. In principle these functions are not completely independent, and one should have $\mathcal{F} \rightarrow \mu$ in the linear limit. We investigate the importance of respecting this limit in [section 5](#). Finally, we remind the reader that all these functions are required to compute the key ingredients of \mathcal{R} (and hence P_{NL}): P_L , $P_{\text{1-loop}}$ and P_{1h} .

The right half of [Figure 1](#) summarises the map from background and Poisson equations to the halo model reaction as described in this section. The left half of the figure will be the focus of the next section.

3 PARAMETRISATIONS

We now move away from the observational end and return to the starting point, the fundamental action of Nature. In particular, here we mostly focus on the Horndeski action given in [Equation 2](#), but the approach can be trivially extended to further generality.

As pointed out, given a specific form of the G_i functions, the explicit functional forms of H , μ , γ_2 , γ_3 and \mathcal{F} can be directly derived. But rather than specifying the full covariant theory, i.e., 4 free functions of space and time, we ultimately wish to parameterise the action’s predictions for cosmological matter clustering in terms of a few free constants.

To do this, we split LSS into three regimes: the *background & linear*, *quasi-nonlinear* and the *nonlinear*. The background, linear and quasi-nonlinear regimes will follow the well studied EFTofDE program ([Gubitosi et al. 2013](#); [Bloomfield et al. 2013](#)). For the nonlinear regime we will consider two different parameterisations. One

is the established nonlinear parameterised post-Friedmannian (nPPF) approach ([Lombriser 2016](#)). The other parametrisation we propose here is phenomenological and is based on some well known screening mechanisms. We begin by parameterising the background & linear regime.

3.1 Background & Linear: Effective field theory of dark energy

Among the methods to generically parameterise beyond- Λ CDM physics on cosmological scales, the methods of Effective Field Theory (EFT) have proven to be particularly useful. It is simply necessary to determine which symmetries one wishes the action to have before constructing various operators out of the fields and derivatives of the fields. One can trust the predictions made with an EFT as long as it is made at an energy scale below the ‘cutoff’ of the theory, beyond which the validity of the EFT breaks down.

While not being an EFT in this strict sense, the EFTofDE is constructed in a similar manner and is capable of describing the dynamics of the cosmological background and perturbations in Horndeski theory in a generic manner. The EFTofDE approach breaks time diffeomorphism invariance of the cosmological background by choosing a particular gauge. By doing this one is able to form a theory out of operators which only respect spatial diffeomorphism invariance.

In constructing the EFTofDE action one begins by foliating space-time with constant-time hypersurfaces. Utilising the complete freedom one has in choosing the coordinates of the theory we can set the scalar field to be only a function of time such that $\phi(x, t) \rightarrow \phi(t)$. In particular, we can choose

$$\phi = t/\kappa^2. \quad (15)$$

This choice is called the *unitary gauge* and in this gauge the scalar field perturbations vanish, being absorbed into the time-time component of the metric. The operators in the EFTofDE are the cosmological perturbations themselves. In the unitary gauge we are free to include operators in the EFT which are only spatially diffeomorphism invariant, such as g^{00} .

Let us denote the normal vector to each spatial hypersurface as

$$n_\mu = -\frac{\partial_\mu \phi}{\sqrt{-(\partial\phi)^2}}. \quad (16)$$

The induced spatial metric of each hypersurface is then given by $h_{\mu\nu} = g_{\mu\nu} + n_\mu n_\nu$. This allows us to include the extrinsic curvature which is given by the projection of the derivative of the normal vector along the the hypersurface, onto the hypersurface $K_{\mu\nu} = h_{\mu\sigma} \nabla^\sigma n_\nu$. With the induced metric, one can also compute the intrinsic curvature of each hypersurface given by the three-dimensional Ricci scalar $R^{(3)}$.

Collecting relevant combinations of the invariants under residual spatial diffeomorphism symmetry gives the EFTofDE action, which is capable of describing the dynamics of the background and linear perturbations of Horndeski theory. The action is given by (see, for example, [Kennedy et al. 2017](#))

$$S_{U,L} = S^{(0,1)} + S^{(2)} + S_M [g_{\mu\nu}, \Psi_m], \quad (17)$$

$$S^{(0,1)} = \int d^4 x \sqrt{-g} \left[\frac{\Omega(t)}{2\kappa^2} R - \Lambda(t) - c(t) \delta g^{00} \right], \quad (18)$$

$$S^{(2)} = \int d^4 x \sqrt{-g} \left[\frac{M_2^4(t)}{2} (\delta g^{00})^2 - \frac{\bar{M}_1^3(t)}{2} \delta K \delta g^{00} - \bar{M}_2^2(t) \left(\delta K^2 - \delta K^{\mu\nu} \delta K_{\mu\nu} - \frac{1}{2} \delta R^{(3)} \delta g^{00} \right) \right]. \quad (19)$$

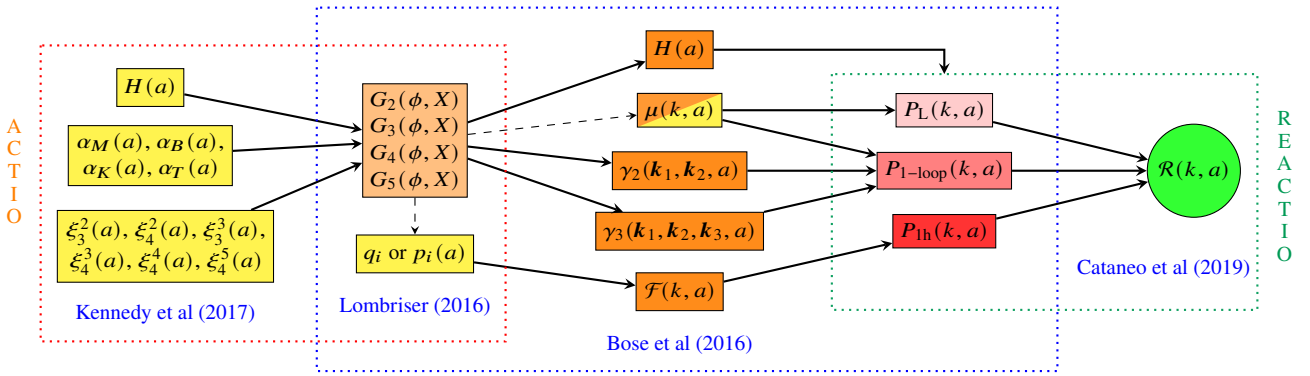


Figure 1. A rough schematic of the map from the Horndeski action in the EFTofDE parametrisation (H, α_i, ξ_i^j) and nonlinear parameterisations (p_i or q_i) to $\mathcal{R}(k, t)$. The yellow rectangles indicate the input functions of time (here parametrised by the scale factor a) or constants. The orange rectangles indicate the modifications to the Poisson equation. $\mu(k, a)$ is bi-coloured indicating we may choose to parametrise it directly instead of starting at the action level. We provide the main sources in the literature for each piece of the map along with a dotted box roughly indicating their associated piece. Note that the solid arrows can only reconstruct G_i to the linear and quasi-nonlinear levels, which can in turn inform choices for p_i . The p_i provide the nonlinear complement in the G_i .

where $S_{U,L}$ represents the action of a Horndeski-universe that describes field dynamics up to the linear level in the matter and velocity perturbations. The $(0, 1, 2)$ represent the order in the perturbed quantities.

In front of each term we include a free function of time called an EFT coefficient, giving a total of six free functions, $\{\Omega(t), \Lambda(t), c(t), M_2^4(t), \bar{M}_1^3(t), \bar{M}_2^2(t)\}$. Once we specify a metric, we also introduce any metric degrees of freedom. For FLRW this is the scale factor a , or equivalently the Hubble parameter $H(a)$. We can then employ the field equation constraints, which in the FLRW are the Friedmann equations

$$0 = \kappa^2(2c - \Lambda + \rho_m) - 3H^2(\Omega + a\Omega'), \quad (20)$$

$$0 = \kappa^2\Lambda + H[aH'(2\Omega + a\Omega') + H(3\Omega + 3a\Omega' + a^2\Omega'')], \quad (21)$$

where we have dropped the time dependence in constituent parameters for compactness, and use the scale factor to parameterise time. A prime denotes a scale factor derivative and ρ_m is the matter density at a . The Friedmann equations reduce the number of free functions describing the background and linear perturbations to five. Solving these equations yields

$$c(a) = -\frac{\rho_m}{2} - \frac{aH[H'(2\Omega + a\Omega') + aH\Omega'']}{\kappa^2}, \quad (22)$$

$$\Lambda(a) = -\frac{H[aH'(2\Omega + a\Omega') + H(3\Omega + 3a\Omega' + a^2\Omega'')]}{\kappa^2}. \quad (23)$$

This means the free functions of the scale factor defining the background and linear theory would be $\{\Omega, H, M_2^4, \bar{M}_1^3, \bar{M}_2^2\}$, which we will refer to as the *M-basis*. We can alternatively write the Hubble function as the solution to

$$H(a) : 0 = (2\Omega + a\Omega')H' + aH\Omega'' + \frac{\kappa\rho_m}{aH} + \frac{2\kappa c}{aH}, \quad (24)$$

if we wish to specify c instead of H for example.

Common in the literature is the *α -basis* $\{H, \alpha_M, \alpha_B, \alpha_K, \alpha_T\}$ which has a clearer physical interpretation of the effects of each function (see, for example, Bellini & Sawicki 2014). We provide the

map between the α - and *M*-bases⁵

$$\alpha_M = \frac{a(M^2)'}{M^2}, \quad (25)$$

$$\alpha_B = -\frac{aH\Omega' + \kappa^2\bar{M}_1^3}{HM^2\kappa^2}, \quad (26)$$

$$\alpha_K = \frac{2c + 4\bar{M}_2^4}{M^2H^2}, \quad (27)$$

$$\alpha_T = -\frac{\bar{M}_2^2}{M^2}, \quad (28)$$

where $M^2 = \Omega \kappa^{-2} + \bar{M}_2^2$. Note that one can alternatively specify M^2 and solve for H .

To end this section, another basis worth considering is the basis introduced in Kennedy et al. (2018): $\{H, M^2, c_s^2, \alpha, \alpha_{B0}\}$ (also see Lombriser et al. 2019), which implicitly assumes $\alpha_T = 0$ (see subsection 4.3 for motivation). This basis allows for some simple priors on the functions that ensure the theory has no ghost or gradient instabilities, i.e., negative energies or imaginary sound speeds. We will refer to this basis as the *s*-basis. The priors to ensure stability on these functions are then simply $M^2, c_s^2, \alpha > 0$, and α_{B0} is constant⁶. The map between the *s*- and α -bases is given by

$$c_s^2 = \frac{2}{\alpha} \left[\frac{\alpha\alpha'_B}{2} + (1 + \alpha_T) \left(1 - \frac{\alpha_B}{2} \right)^2 - \left(1 + \alpha_M - \frac{\alpha H'}{H} \right) \left(1 - \frac{\alpha_B}{2} \right) + \frac{\rho_m}{2H^2M^2} \right], \quad (29)$$

$$\alpha = \alpha_K + \frac{3}{2}\alpha_B^2, \quad (30)$$

where c_s is the speed of sound, while $\alpha_{B0} = \alpha_B(a = 1)$ is the boundary condition (α_B 's value today) specified to solve the differential equation given by Equation 29.

In what follows we will stick with the α -basis and implement this as the default basis in the accompanying code **ACTio et ReACTio**. We provide the explicit form of the linear modification to the Poisson

⁵ Note the factor of ‘ $-1/2$ ’ difference in α_B between our expression and that of EFTCMB (Frusciante et al. 2016) or Kennedy et al. (2018), for instance.

⁶ We note that this basis does not ensure the absence of a tachyonic instability (Gspone & Noller 2022).

equation in this basis in [subsection A1](#). We leave it to the user to perform the transformation from their preferred basis to the α -basis, and provide an accompanying notebook [GtoPT.nb](#) that performs some of these transformations.

3.2 Quasi-nonlinear: Covariant theory map

To fully specify the halo model reaction, we need to go beyond the linear matter perturbations. In particular, we also require the 2nd and 3rd order density perturbations to solve for the 1-loop power spectrum entering \mathcal{R}_{SPT} in [Equation 10-11](#). This requires us to expand to fourth order in the metric perturbation δg^{00} and extrinsic curvature $\delta K^{\mu\nu}$ in [Equation 17](#). This has been done in [Cusin et al. \(2018b\)](#) and has been used to calculate the 1-loop spectrum in [Cusin et al. \(2018a\)](#). Further, in [Kennedy et al. \(2017\)](#) the authors relate the EFTofDE functions up to a given order to the corresponding covariant theory's Lagrangian G_i functions as

$$G_i(\phi, X) = g_i(\phi, X) + \Delta G_i(\phi, X), \quad (31)$$

where $g_i, i \in \{2, 3, 4, 5\}$, are well-defined functions of ϕ, X and the lower order EFTofDE parameters, e.g., $\{H, \alpha_M, \alpha_B, \alpha_K, \alpha_T\}$. The other terms are given as

$$\Delta G_{2,3} = \sum_{n>2} \xi_n^{(2,3)}(\phi) (1 + X \kappa^4)^n, \quad (32)$$

$$\Delta G_{4,5} = \sum_{n>3} \xi_n^{(4,5)}(\phi) (1 + X \kappa^4)^n, \quad (33)$$

where ΔG_i are higher order corrections to the covariant action and $\xi_n^i(\phi)$ are higher order EFTofDE functions, X again being the scalar field canonical kinetic energy term.

A particular covariant theory is specified once ξ_n^i are given for all $n \in \mathbb{N}$, but if we truncate at some order n_t , we specify the subset of Horndeski theories which are identical on scales described by the EFTofDE up to $\xi_{n_t}^i$. Up to 3rd order in the matter density perturbation, we introduce 6 new functions with $n_t = 4$. Together with the background and linear order functions, this gives a total of 11 free functions of time for the quasi-nonlinear scales. The G_i given in [Equation 31](#) can then be related to μ, γ_2 and γ_3 by the map provided in the Appendices of [Bose & Koyama \(2016\)](#); [Takushima et al. \(2015\)](#).

In [section A](#) we provide the map between the 5 linear EFTofDE functions in the α -basis and the linear modification to the Poisson equation, μ , used in [Equation 12](#). The 2nd and 3rd order functions γ_2 and γ_3 (see [Equation 14](#)) are significantly more complicated but can be derived by using the map from the EFTofDE to $G_i(\phi, X)$ provided in [Kennedy et al. \(2017\)](#) and then the $G_i(\phi, X)$ to γ_2 & γ_3 given in [Bose & Koyama \(2016\)](#). The map, although not reproduced here in full, is given in detail in a [Mathematica](#) notebook provided in the [ACTio et ReACTio](#) repository, [GtoPT.nb](#). This being said, in [section 4](#) we give support for the omission of γ_2 and γ_3 in the calculation of \mathcal{R} for moderate to low modifications to gravity, and given the additional degrees of freedom we will introduce in the nonlinear regime.

Having specified a route between the Horndeski action of nature and the linear and 1-loop power spectra, $P_L(k, a)$ & $P_{1\text{-loop}}(k, a)$, we now look at two methods of parameterising clustering in the highly nonlinear regime, characterised by the 1-halo term, $P_{1\text{h}}(k, a)$. This will then specify a full parameterisation of the halo model reaction \mathcal{R} , and consequently the nonlinear power spectrum, $P_{\text{NL}}(k, a)$.

3.3 Nonlinear

The effects of modified gravity on the nonlinear cosmic structure formation are captured by the effective deviation \mathcal{F} from the gravitational constant in the nonlinear Poisson equation given in [Equation 13](#) and the cosmological background evolution. Specifically, the modified Poisson equation alters the evolution equation for the halo top-hat radius R_{TH} (see, for example, [Schmidt et al. 2009](#)). This quantity gives an estimate for δ_{NL} , needed to compute the 1-halo power spectrum. Here we discuss two parameterisations of \mathcal{F} .

3.3.1 Nonlinear parametrised post-Friedmannian framework

Following the nPPF approach of [Lombriser \(2016\)](#), the effective gravitational coupling for generic screening mechanisms and other suppression effects can be decomposed as a function of scale r

$$1 + \mathcal{F}(a, r) = A + \sum_i^{N_0} B_i \prod_j^{N_i} \mathcal{F}_{ij}, \quad (34)$$

where \mathcal{F}_{ij} are some transition functions encapsulating screening or other suppression effects such as a Yukawa suppression. N_0 and N_i characterise their respective number. In the fully screened limit, the effective coupling reduces to A , typically unity, whereas it becomes B_i in the fully unscreened limit, matching linear theory. To parameterise these transitions, [Lombriser \(2016\)](#) adopted a generalised form of the Vainshtein screening effect in the DGP braneworld model ([Dvali et al. 2000](#))

$$\mathcal{F} \sim b \left(\frac{r}{r_{\text{scr}}} \right)^{a_f} \left\{ \left[1 + \left(\frac{r_{\text{scr}}}{r} \right)^{a_f} \right]^{1/b} - 1 \right\}, \quad (35)$$

where r_{scr} denotes the screening scale, which in general can be time, mass, and environment dependent. The parameter a_f (not to be confused with the scale factor) determines the radial dependence of the coupling in the screening limit along with b that characterises an interpolation rate between the screened and unscreened limits.

Screening effects such as the chameleon ([Li & Efstathiou 2012](#); [Khoury & Weltman 2004](#); [Lombriser et al. 2014](#)) symmetron ([Hinterbichler & Khoury 2010](#); [Taddei et al. 2014](#)), k-mouflage ([Babichev et al. 2009](#); [Brax & Valageas 2014](#)), and Vainshtein ([Vainshtein 1972](#); [Schmidt et al. 2010](#); [Dvali et al. 2000](#)) mechanisms as well as other suppression effects such as the linear shielding mechanism ([Lombriser & Taylor 2015b](#)) or Yukawa suppression, can be analytically mapped onto [Equation 35](#) by matching expressions in the limits of large and small r and $r \rightarrow r_{\text{scr}}$. The relevant expressions may be found in [Lombriser \(2016\)](#). It is worth highlighting that the parameters of [Equation 35](#) for a given screening model may in principle be directly read off from [Equation 2](#) by employing the scaling method of [McManus et al. \(2016\)](#) (also see [Renevey et al. 2020](#)) and counting the powers of second and first spatial derivatives and the scalar field potential. Note that the parameter b may be understood as the choice of transition template used to approximately cast the screening effect into. Alternatively to [Equation 35](#), one could also adopt other transition functions such as a hyperbolic tangent, a sigmoid or an error function as we will propose in [subsubsection 3.3.2](#). For DGP, the choice of [Equation 35](#) with $b = 2$ becomes exact.

To implement [Equation 35](#) in the spherical collapse model, one replaces $r/r_{\text{scr}} \rightarrow y/y_{\text{scr}}$, where y is the normalised top-hat radius ([Equation B4](#)). A single general element $N_0 = N_1 = 1$ can then be described by seven parameters (or functions) p_{1-7} in addition to $p_0 = A$ (typically = 1). The first three, p_{1-3} , determine a_f, b , and B . The other four are used to generally capture possible time, mass, and

environmental dependencies of the dimensionless screening scale, which can be modelled as (Lombriser 2016)

$$y_{\text{scr}} = p_4 a^{p_5} (2G_N H_0 M_{\text{vir}})^{p_6} \left(\frac{y_{\text{env}}}{y_h} \right)^{p_7}, \quad (36)$$

where y_h and y_{env} refer to the normalised radii of the the halo and the environment respectively, H_0 is the Hubble constant and M_{vir} is the virial mass of the halo⁷. In this way, we can simplify Equation 35 to (Lombriser 2016)

$$\mathcal{F}_{\text{nPPF}} = p_1 p_2 \frac{(1 + s^{a_f})^{\frac{1}{p_1}} - 1}{s^{a_f}}, \quad (37)$$

where

$$a_f = \frac{p_1}{p_1 - 1} p_3 \quad (38)$$

and $s = y_{\text{scr}}/y_h$. Note we have set $p_0 = 1$. The parameters p_{1-7} can be computed from theory and in many cases take on trivial values (see subsection B2). It is worth highlighting here that the nPPF formalism has also been implemented in N -body simulations and cast into Fourier space (Hassani & Lombriser 2020), where it was shown to accurately match simulations of exact model implementations.

Finally, we consider the large, linear scale limit of \mathcal{F} . Equation 39 provides a parametrised function for the screening regime, where we have a transition to GR from some large scale modification. In this form, it does not capture any additional effects coming from say Yukawa suppression, typical of chameleon theories. Such phenomena may become relevant for the spherical collapse calculation at early times or for very large halo masses. In order to correctly capture this, we could either model the Yukawa suppression as another transition cast into Equation 37 or simply augment Equation 37 with the linear modification $\mu(k, a)$ as

$$\mathcal{F}_{\text{nPPF}} = p_1 p_2 \frac{(1 + s^{a_f})^{\frac{1}{p_1}} - 1}{s^{a_f}} \times (1 - \mu(\hat{k}, a)). \quad (39)$$

In this case we also need to perform the Fourier transform of $\mu(\hat{k}, a)$, which is non-trivial. As a first order approximation, we parametrise this with a simple scaling of the inverse of the comoving initial top-hat radius R_{th} as

$$\hat{k} = \frac{10^{p_8}}{a^2 y_h R_{\text{th}}}, \quad (40)$$

where the dimensionless constant p_8 calibrates the Yukawa suppression. The Fourier transform can be made more sophisticated (see, for example, Hassani & Lombriser 2020) but in section 5 we find the impact of Yukawa suppression is negligible for the $f(R)$ models we consider, and so only include this augmentation for completeness. Further, Equation 39 would only be meaningful for a non-trivial scale dependent $\mu(k, a)$. For scale-independent theories one can absorb the scaling provided by $\mu(a)$ in the $p_2(a)$ parameter of Equation 37.

3.3.2 Phenomenological parameterisation

With its full freedom, the nPPF parameterisation is a very flexible way of modelling the nonlinear scales. It is able to capture various specific covariant theories exactly or to high accuracy (see subsection B2 and section 5), and given a covariant theory, say from the

⁷ Note that in ReACT we use the initial comoving top-hat radius, R_{th} (see subsection B4), as an input parameter instead of mass, related as $M_{\text{vir}} = 4\pi\bar{\rho}_{\text{m},i}(1 + \delta_i)(a_i R_{\text{th}})^3/3 \approx 4\pi\Omega_{\text{m},0}\rho_{\text{crit}}R_{\text{th}}^3/3$ with the critical density ρ_{crit} and $1 + \delta_i \approx 1$.

Horndeski class, we can map its nonlinear Poisson modification to the p_i parameters. On the other hand, if we remain agnostic about the covariant theory, 8 additional parameters, some of which may also be time dependent, poses computational issues as well as degrades the amount of cosmological and gravitational information we can extract due to degeneracies between these nuisance and the physical parameters of interest.

With this in mind, we propose the following general and reduced parameterisation of \mathcal{F} based on the error function (Erf). We have found this mimics the general profile of the effective gravitational constant in various modified gravity theories. Essentially we wish to capture a basic transition from unscreened to screened regimes. The simple form we adopt is given by

$$\mathcal{F}_{\text{Erf}} = \text{Erf}[a y_h 10^{\tilde{J}}] \times (1 - \mu(\hat{k}, a)), \quad (41)$$

where as in the nPPF case, we use

$$\hat{k} = \frac{10^{q_4}}{a^2 y_h R_{\text{th}}}, \quad (42)$$

and

$$\tilde{J} = q_1 - q_2 \log(R_{\text{th}}) + q_3 \log(a y_{\text{env}}). \quad (43)$$

μ is the linear modification to gravity. In the EFTofDE parameterisation μ is given in Equation A1, but this can also be parametrised more generally (see, for example, Silvestri et al. 2013; Kennedy et al. 2018; Srinivasan et al. 2021).

The Erf model introduces 4 free constants:

- q₁**: This parametrises the screening scale and goes as its inverse.
- q₂**: This gives the halo mass dependency of the screening scale.
- q₃**: This gives the environment dependency of the screening scale.
- q₄**: This calibrates any existing Yukawa suppression scale.

The time dependence of \mathcal{F}_{Erf} is fixed and so for a specified cosmology and set of EFTofDE parameters, we only need to adjust the constants $\{q_1, q_2, q_3, q_4\}$. To provide some insight, we note the following limits

$$\lim_{q_1 \rightarrow \infty} 1 + \mathcal{F}_{\text{Erf}} = \mu \rightarrow \text{Unscreened limit}, \quad (44)$$

$$\lim_{q_1 \rightarrow -\infty} 1 + \mathcal{F}_{\text{Erf}} = 1 \rightarrow \text{GR limit}, \quad (45)$$

$$\lim_{q_2, q_3 \rightarrow 0} 1 + \mathcal{F}_{\text{Erf}} \rightarrow \text{Vainshtein type models}, \quad (46)$$

$$\lim_{q_3 \rightarrow 0} 1 + \mathcal{F}_{\text{Erf}} \rightarrow \text{k - camouflage type models}, \quad (47)$$

$$q_3 > 0 : 1 + \mathcal{F}_{\text{Erf}} \rightarrow \text{chameleon type models}, \quad (48)$$

where we refer to the main types of screening mechanisms typical of scalar-tensor theories (see subsubsection 3.3.1). Note that all parameters lose their meaning as $\mu(k, a) \rightarrow 1$, which in the EFTofDE case is when the relevant parameters assume their GR values.

Given this, we can take q_2 and q_3 to be positive. Being exponents of the top-hat radius and environment parameter, they are also not expected to be very large, and as we will see in section 5, they turn out to be $\mathcal{O}(1)$. Further, since in the GR limit $\mu \rightarrow 1$, and so $\mathcal{F}_{\text{Erf}} \rightarrow 0$ irrespective of the value of q_1 , we can also take q_1 to be positive. We also find q_1 to be an $\mathcal{O}(1)$ parameter.

Parameter q_4 , which calibrates the Yukawa suppression scale, is generally only relevant for theories where the linear growth factor, or Poisson modification μ , is scale-dependent. As we will show in subsection 5.2, q_4 does not appear to be relevant for the scales associated with spherical collapse. We note q_4 can in principle take on negative values, pushing the Yukawa suppression to smaller scales. As $q_4 \rightarrow \infty$ the Yukawa suppression scale also goes to infinity. We leave its relevance for more general theories for a future work.

We provide a **Mathematica** notebook, `Nonlinear.nb`, with all the forms of \mathcal{F} considered in this paper along with comparisons.

Finally, the left half of [Figure 1](#) summarises the map from the parametrised action, together with additional parameters, to the Poisson equation modifications as described in this section, completing the map from action to reaction.

4 APPROXIMATIONS AND OVERVIEW

We have outlined a map that goes from the parameterised action of nature and structure formation $\{H\}_b, \{\alpha_M, \alpha_B, \alpha_K, \alpha_T\}_L, \{\xi_3^2, \xi_4^2, \xi_3^3, \xi_4^3, \xi_4^4, \xi_4^5\}_{\text{QNL}} \& \{p_1, p_2, p_3, p_4, p_5, p_6, p_7, p_8\}_{\text{NL}}$ or $\{q_1, q_2, q_3, q_4\}_{\text{NL}}$ to the nonlinear effects on the power spectrum $\mathcal{R}(k, a)$, where ‘b’ stands for background, ‘L’ for linear, ‘QNL’ for quasi-nonlinear and ‘NL’ for nonlinear. A schematic of this map is given in [Figure 1](#). An important point worth stressing is that our nonlinear parametrisations are completely general, and not specific to the Horndeski class of theories. They do however rely on $\mu(k, a)$, which one can always choose to parametrise in a model independent way.

Considering the Horndeski class for concreteness, the EFTofDE and nonlinear parametrisations constitute a very large set of arbitrary functions of time and constants. Despite it being significantly less than the infinite number of theories contained within the Horndeski class, it is still arguably too many for statistical data analyses, both on computational and scientific grounds. Thankfully, as we will shortly motivate, these sets can be yet reduced significantly.

To reduce or optimise the parameter space, we consider the following:

- (1) We assume the quasi-static approximation (QS) for all perturbative calculations (see [Sawicki & Bellini 2015](#); [Pace et al. 2021](#), for example).
- (2) We assume $\gamma_2 = \gamma_3 = 0$.
- (3) Observational and theoretical constraints.
- (4) Time parameterisations of EFTofDE functions, $\alpha_i(a)$.
- (5) The parameterised nPPF (see [Equation 39](#)) or phenomenological (see [Equation 41](#)) form of \mathcal{F} is flexible enough to capture general modifications to gravity.

In this section we will motivate approximations (1) - (4) with direct reference to the accompanying code `ACTio` et `ReACTio`. Assumption (5) will be addressed separately in [section 5](#).

4.1 Quasi-static approximation

We begin by noting that the QS in linear theory can be easily avoided by using a Boltzmann code such as EFTCAMB ([Hu et al. 2014](#); [Raveri et al. 2014](#)) to calculate the linear input spectrum or transfer function⁸. This option is available in our code, but the default setting assumes a Λ CDM linear spectrum or transfer function at $z = 0$ and rescales it using the internally calculated growth functions of the desired theory. This is done using the linear form of [Equation 12](#) (see [Equation A1](#)) which assumes the quasi-static approximation. Being able to use a Λ CDM linear spectrum enhances the computational

efficiency of our code as it avoids a call to EFTCAMB. EFTCAMB is significantly slower than CAMB ([Lewis et al. 2000](#)), which already takes $\mathcal{O}(1)$ seconds to produce a linear spectrum. In this case one can also use a linear spectrum emulator like CosmoPower ([Spurio Mancini et al. 2022](#)) or bacco ([Aricò et al. 2021](#)), which takes $\mathcal{O}(0.1)$ seconds to produce the linear spectrum.

Given the utility in using the QS, we want to get an idea of its validity. In [Figure 2](#) we show the effects of the QS at $z = 0$ and $z = 1$ for models with non-zero α_K and α_B (KGB [Deffayet et al. 2010](#)), on the nonlinear spectrum as given by [Equation 3](#). We use the halofit ([Takahashi et al. 2012](#)) formula for $P_{\text{NL}}^{\text{pseudo}}$ and assume a Λ CDM background expansion, $H(a) = H_{\Lambda\text{CDM}}(a)$ as well as no screening effects, i.e., $\mathcal{F} = \mu - 1$ and $\gamma_2 = \gamma_3 = 0$.

We find that the QS is valid for these mild to moderate parameter choices on scales of $k \geq 0.1h/\text{Mpc}$. Upcoming surveys will probe scales larger than this which may be an issue. Taking into account cosmic variance assuming a galaxy survey volume similar to the effective volume of forthcoming surveys, $V_{\text{eff}} = 20 \text{ Gpc}^3/h^3$ ([Laureijs et al. 2011](#); [Aghamousa et al. 2016](#); [Blanchard et al. 2020b](#)), the QS is still a sub-dominant source of error for even extreme choices of α_B and α_K (see [subsection 4.3](#)). Note that time derivatives of the fields drop out from the calculation of μ for $k \rightarrow \infty$ in Horndeski theories ([Lombriser & Taylor 2015a](#); [Pace et al. 2021](#)). We note at small scales, modelling inaccuracies and shot noise errors will arguably dominate any inaccuracies incurred from using the QS.

We do however warn that the QS begins to break significantly for beyond Horndeski theories ([Lombriser & Taylor 2015a](#)). For large modifications to GR within Horndeski, we advise comparing the resulting nonlinear spectrum with and without the QS against the predicted errors on the specific data that is being analysed. Further, we have implemented the following necessary condition for the QS to hold in our code ([Peirone et al. 2018](#))

$$\frac{k}{aH(a)} > c_s^2(a), \quad (49)$$

where c_s^2 is given by [Equation 29](#), with its violation producing a warning prompt.

4.2 $\gamma_2 = \gamma_3 = 0$ approximation

We begin by noting that setting $\gamma_2 = \gamma_3 = 0$ implies we have $R_{\text{SPT}} \approx 1$ in [Equation 10](#) as the 1-halo terms are subdominant. This forces the argument of the logarithm in [Equation 9](#) to be very close to unity, giving a very large k_{star} . Effectively, this is the same as setting $\mathcal{E} = 1$ in [Equation 6](#). This is the choice we take when adopting this approximation. We should remark that simply setting $\gamma_2 = \gamma_3 = 0$ leaves one slightly sensitive to the k_{star} correction through the 1-halo terms and consequently on the particular choice of halo mass function.

Using the exact forms of γ_2 & γ_3 as described in [subsection 3.2](#) is a big challenge. This is primarily for computational reasons as it involves numerical time derivatives. Smoothness of such derivatives is difficult to ensure and can affect results. In particular, the exponential dependence of \mathcal{R} on k_{\star} (see [Equation 4](#)) makes it very sensitive to inaccuracies in the 1-loop calculation. Further, the full map to γ_2 & γ_3 from the EFTofDE would increase computational time significantly, degrading our code’s ability to perform statistical analyses on data.

To test the impact of setting $\gamma_2 = \gamma_3 = 0$ we compare [Equation 4](#) with and without these terms switched on for two different theories of gravity, DGP and the Hu-Sawicki $f(R)$ model ([Hu & Sawicki 2007](#)). The former is an instance of derivative or Vainshtein screening and

⁸ The QS can be partly circumvented in the nonlinear regime, [Equation 39](#) and [Equation 41](#), by also using the prediction of $\mu(k, a)$ taken from say EFTCAMB.

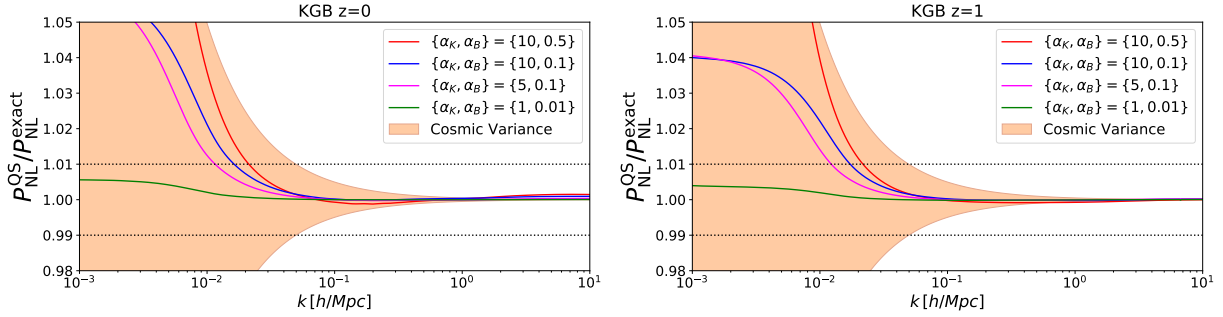


Figure 2. Ratio of the quasi-static approximated (QS) nonlinear spectrum to the exact calculation. We show the results for four EFTofDE models with $\{\alpha_K, \alpha_B\}$ non-zero and all other α parameters set to 0 and a Λ CDM background expansion, at $z = 0$ (left) and $z = 1$ (right). The exact calculation uses Equation 4 with an EFTCMB linear spectrum while the QS uses Equation 4 with a rescaled Λ CDM linear spectrum using the modified growth equations, making use of Equation A1. The orange band represents the error coming from cosmic variance assuming an effective survey volume of $V_{\text{eff}} = 20 \text{ Gpc}^3/h^3$. We assume $\mathcal{F} = \mu - 1$ and $\mathcal{E} = 1$ in all nonlinear computations. The dotted lines mark 1% deviations which is an optimistic estimate on the modelling errors of the halo model reaction framework.

the latter of potential or chameleon screening, covering two main types of screening mechanism.

This comparison is shown in Figure 3. We find that in the case of DGP, the correction coming from the 1-loop computation is negligible for small and moderate modifications to GR at all scales. On the other hand, the corrections to the $f(R)$ theory can be up to 1.5% at $z = 0$ for moderate modifications to GR. This may be acceptable if these inaccuracies can be partially absorbed into the nonlinear degrees of freedom. We explore this in section 5.

4.3 Observational and theoretical constraints

Firstly, we want to eliminate a range of α -parameter values that leads to two pathological instabilities: ghost (i.e., negative kinetic energy) and gradient (i.e., imaginary speed of sound). These constraints for the Horndeski theories were first derived in De Felice & Tsujikawa (2012). In terms of the α -functions, Bellini & Sawicki (2014) found that the stability of the background requires

$$\alpha > 0, \quad c_s^2 \geq 0, \quad (50)$$

from Equation 29 and Equation 30 for scalar modes, and

$$M^2 > 0, \quad c_T^2 = 1 + \alpha_T \geq 0 \quad (51)$$

for tensor modes of perturbations. An additional theoretical constraint is the stability of scalar modes in the presence of gravitational waves of large amplitude, for instance, sourced by massive binary systems (Creminelli et al. 2020). Mapped to the parameterisation used in this work this requires the following bound (Noller 2020):

$$|\alpha_M + \alpha_B| \lesssim 10^{-2}. \quad (52)$$

Previously, it was argued that the constraining power of upcoming cosmological surveys will allow us to pin down the α -parameters at the $\mathcal{O}(0.1)$ -level (e.g., Frusciante et al. 2019). For the condition above this implies that $\alpha_M \approx -\alpha_B$. However, in such forecasts nonlinear scales were ignored with a typical highest mode around $k_{\text{max}} \approx 0.15 \text{ h Mpc}^{-1}$. We speculate that this constraint may be improved upon by inclusion of the nonlinear scales. Therefore, in our code we treat α_B and α_M independently.

Secondly, one may consider that the new physics should not modify the speed of gravitational wave propagation (Lombriser & Taylor 2016; Abbott et al. 2017; Lombriser & Lima 2017; Creminelli & Vernizzi 2017; Ezquiaga & Zumalacárregui 2017; Baker et al. 2017; Sakstein & Jain 2017; Battye et al. 2018; de Rham & Melville 2018;

Creminelli et al. 2018), and so $\alpha_T = \bar{M}_2^2 = 0$. This luminosity condition has been argued to not be as clear cut a constraint through EFT considerations (de Rham & Melville 2018; Baker et al. 2022) as well as through the positivity bounds from high energy physics (de Rham et al. 2021), so in our code we keep the α_T dependence in μ . Subluminality, stated in the former references, follows from the existence of a Wilsonian UV completion (Adams et al. 2006) and dependence on the theory's 'cutoff' scale. From Equation 29 it can be seen that subluminality of scalar modes is guaranteed for large values of α_K , while for tensor modes subluminality requires $\alpha_T < 0$. Superluminality, stated in de Rham et al. (2021), is a consequence of the positivity bounds for scattering between scalar and matter fields. Such positivity bounds require a unitary, causal, local UV completion of our low-energy EFT theory. However, superluminality does not necessarily result in causal paradoxes (Babichev et al. 2008; Burrage et al. 2012). In general, the notion of causality in terms of the low-energy EFT is a rather subtle topic (for instance, see de Rham & Tolley 2020; Reall 2021).

Thirdly, in the QS α_K does not enter the equations of motion (Bellini & Sawicki 2014). Therefore, it is completely unconstrained in our approach, or for any model with $c_s^2 \approx 1$. However, in the exact computation α_K affects only the largest scales (see Figure 2), which are dominated by cosmic variance. This can be a motivation to not consider α_K in data analyses, leaving only α_M and α_B in a 'bare-bones' case. We do not impose any of these reductions in our code and leave it to the user to specify well motivated priors on the full set of EFTofDE parameters in their analyses.

Lastly, we note that there are a host of data driven constraints that one can put on the EFTofDE parameters (Huang 2016; Bellini et al. 2016; Noller & Nicola 2019a; Noller & Nicola 2019b; Spurio Mancini et al. 2019; Melville & Noller 2020; Noller 2020; de Rham et al. 2021). Such constraints strongly depend on the imposed theoretical priors and time-dependent parameterisation of the α -functions (see subsection 4.4). However, they all agree that the uncertainties and values of the α -parameters are of order $\mathcal{O}(0.1)$. The future CMB and LSS surveys promise to improve the constraints up to at least one order of magnitude $\sigma(|\alpha_i|) \sim \mathcal{O}(0.01)$ (see, for example, Abazajian et al. 2016). One may also assume a Λ CDM background, well motivated by CMB data (e.g., Aghanim et al. 2020), and so set

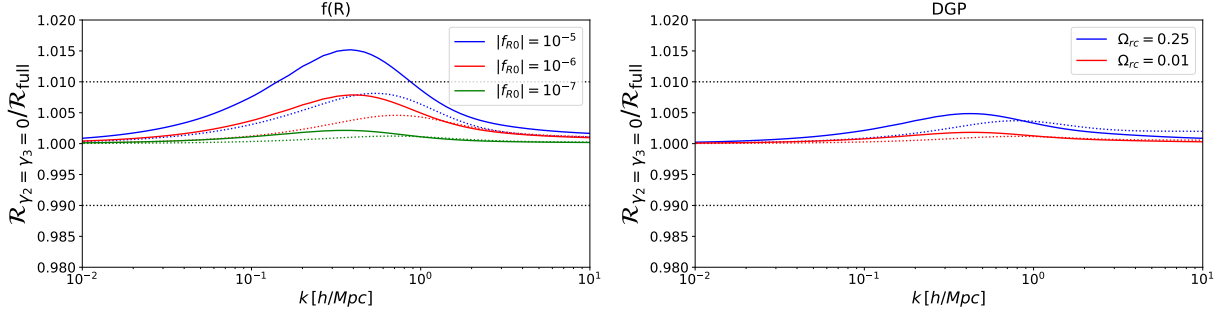


Figure 3. Ratio of the approximated reaction to the full calculation. The approximation assumes $\mathcal{E} = 1$ in Equation 6 which is approximately equivalent to no higher order perturbative, screening terms i.e. $\gamma_2 = \gamma_3 = 0$. We show Hu-Sawicki $f(R)$ gravity on the left and the normal branch of DGP on the right for varying modifications to GR. For $f(R)$ we show predictions for when the model parameter takes the value of $|f_{R0}| = 10^{-5}$ (moderate modification, blue), $|f_{R0}| = 10^{-6}$ (low modification, red) and $|f_{R0}| = 10^{-7}$ (very low modification, green). For DGP we show predictions for when the model parameter is $\Omega_{rc} = 0.25$ (moderate modification, blue) and $\Omega_{rc} = 0.01$ (low modification, red). We also show the comparison over two redshifts, $z = 0$ (solid lines) and $z = 1$ (dotted lines).

Table 1. Theoretical and observational constraints on α -parameters from references in the right column. Theoretical constraints are coming from low-energy (EFT) and high-energy (positivity bounds) physics. Note that α_K is not constrained by data, hence the subluminality condition does not impose any constraining power on the scalar mode perturbations. Also note the contradiction in the condition for GW propagation: subluminal versus superluminal speed. The positivity bounds do not hold in general, they are derived for a quadratic subclass of Horndeski theories with $G_3 = G_5 = G_{5,X} = 0$ in Equation 2. Data driven constraints strongly depend on the imposed theoretical priors and time-dependent parametrization of α -functions. Here we mention only two prior-independent observational constraints.

		scalar	tensor	
Low Energy	no ghost	$\alpha_K + \frac{3}{2} \alpha_B^2 > 0$	$M^2 > 0$	Bellini & Sawicki (2014)
	gradient stability	$c_S^2 \geq 0$	$\alpha_T \geq -1$	de Rham & Melville (2018)
	(sub)luminality	large α_K	$\alpha_T \leq 0$	Creminelli et al. (2020)
High Energy	no GW-induced instability	$ \alpha_M + \alpha_B \lesssim 10^{-2}$		
	scalar-scalar scattering	$\alpha_B \leq \frac{2\alpha_T}{1+\alpha_T}$		Melville & Noller (2020)
Data	scalar-matter scattering	$\alpha_T \geq 0$		de Rham et al. (2021)
	GW propagation speed	$ \alpha_T \leq 10^{-15}$		Abbott et al. (2017)
	CMB and LSS	$ \alpha_M , \alpha_B \leq O(0.1)$		Spurio Mancini et al. (2019)

$H(a) = H_{\Lambda\text{CDM}}(a)$ ⁹. We summarize the constraints discussed above in Table 1.

4.4 Parameterising time dependence

Here, we look at how one can parameterise the time dependence of the EFTofDE functions. To first order this can be approximated by a Taylor expansion, $\theta_i(a) \approx \theta_{i,0} + \theta_{i,p}(1-a)$, leaving at least 6 free constants characterising deviations from ΛCDM . In typical data analyses, only a 1-parameter time dependence is considered. For example, in Noller & Nicola (2019a) the authors consider the following three parameterisations for the α_i , $i \in \{M, B, K, T\}$

$$(1) : \alpha_i(a) = c_i \Omega_\Lambda(a), \quad (53)$$

$$(2) : \alpha_i(a) = c_i a, \quad (54)$$

$$(3) : \alpha_i(a) = c_i a^{n_i}, \quad (55)$$

where c_i and n_i are free constants and $\Omega_\Lambda(a)$ is the ΛCDM cosmological constant energy density fraction as a function of time. For a comprehensive list of various other time parameterisations see Appendix B of Frusciante & Perenon (2020). These all draw on the motivation that modifications should only become relevant at late times. In our code, the default is set to (2) for all α_i . We note that

⁹ Our code defaults to this assumption, but there is the option to parameterise the background too.

such parametrisations may exclude well-known theories as shown in Kennedy et al. (2018), which motivated the s -basis introduced in subsection 3.1.

We can also adopt similar parametrisations for the background $H(a)$, but a more general choice would be for example the Chevalier-Polarski-Linder (CPL) parametrisation (Chevallier & Polarski 2001; Linder 2003), which parametrises the dark energy equation of state $w(a)$ in terms of two free constants, $\{w_0, w_a\}$ as

$$w(a) = w_0 + w_a(1-a), \quad (56)$$

which gives the following form for $H(a)$

$$H^2(a) = H_0^2 \left(\Omega_{m,0} a^{-3} + \Omega_\Lambda e^{-3 \int (1+w(a)) d \log a} \right). \quad (57)$$

4.5 Parametrisation of \mathcal{F}

The nPPF form for \mathcal{F} given in Equation 39 captures dependencies of the nonlinear modification to the Poisson equation on the relevant variables, namely $\{y_h, a, M_{vir}, y_{env}\}$. Being motivated by the form of \mathcal{F} in DGP (Equation B1), it can recover the DGP form given appropriate choices for p_i albeit with a non-trivial dependency of p_2 on a (see Equation B9). Equation 39 becomes approximate when moving beyond DGP. On the other hand, the Erf form, Equation 41, is completely phenomenological and is an approximation even in DGP.

Note that the nPPF is also more directly relatable to specific actions

Table 2. A maximal, reduced and minimal set of parameters needed for a comprehensive nonlinear power spectrum analysis of the unrestricted theory space of Equation 2, together with a proposed minimal set for more general theories. The Horndeski minimal set assumes $\alpha_T = \alpha_K = 0$ and Equation 43, while the maximal and the reduced assume full freedom of Equation 39. Both reduced and minimal assume $\gamma_2 = \gamma_3 = 0$. The totals show the number of free functions of time plus any free constants. We note q_4 and p_8 are found in section 5 to be likely irrelevant for the 1-halo computation, and so we do not consider them in the reduced or minimal cases. We also note very tight constraints on $\alpha_B - \alpha_M$ (see subsection 4.3) relevant to the minimal case.

	Maximal	Reduced	Minimal (Horndeski)	Minimal (general)
Background	$H(a)$	$H(a)$	$H(a)$	w_0, w_a
Linear	$\alpha_M(a), \alpha_B(a), \alpha_K(a), \alpha_T(a)$	$\alpha_M(a), \alpha_B(a), \alpha_K(a), \alpha_T(a)$	$\alpha_M(a), \alpha_B(a)$	γ
Quasi-nonlinear	$\xi_3^2(a), \xi_4^2(a), \xi_3^3(a), \xi_4^3(a), \xi_4^4(a), \xi_4^5(a)$	-	-	-
Nonlinear	$p_{1-7}(a) + p_8$	$p_{1-7}(a)$	q_1, q_2, q_3	q_1, q_2, q_3
Total	18+1	12	3 + 3 constants	6 constants

and gravity models, in which case its degrees of freedom can be significantly restricted. It is thus far more suitable when particular models are being targeted for analysis. The Erf model on the other hand is completely general and has no direct relation to specific actions of gravity. It is thus more suitable when no specific model is being targeted and we want to place constraints on general models of gravity. In section 5 we test these two approximations in both DGP and $f(R)$ gravity.

4.6 Overview

With all these approximations and constraints, the arguable minimal parameter space characterising deviations to Λ CDM is 3 free functions of time and 4 constants. Without approximations or constraints, the maximal is 18 free functions of time and a constant. Of course we can also find intermediate reduced sets, such as using the nPPF but with $\gamma_2 = \gamma_3 = 0$. Given we need to parameterise these functions of time, the maximal set is currently an unfeasible parameter space to probe comprehensively, both in terms of data processing as well as parameter degeneracies which limits the amount of useful physical information one can extract from the data.

Finally, we have focused on the Horndeski class of models, but one can extend this to larger generality by considering for example the growth index γ parametrisation for $\mu(a)$ (Peebles 1980; Linder & Cahn 2007) (explicitly, see Eq. 47 of Kennedy et al. 2018) and Equation 57 for $H(a)$. Combined with the Erf model, this would constitute a minimal set of 6 free constants for general modifications to Λ CDM. This minimal model-independent parametrisation has also been implemented into the code.

We summarise these parameterisations in Table 2.

5 TESTING THE NONLINEAR PARAMETERISATIONS

In this section we compare the predictions for the halo model reaction \mathcal{R} , using the various nonlinear parameterisations of modifications to the Poisson equation outlined in subsection 3.3, to the exact solutions within Hu-Sawicki $f(R)$ gravity and DGP. These exact solutions have in turn been themselves compared to full N -body simulations in other works (see Cataneo et al. 2019, for example), exhibiting $O(1)\%$ agreement. These models cover a fair range of theoretical and phenomenological features typical of modified gravity and dark energy models, making them good representatives and test cases.

We look to test predictions for \mathcal{R} using Equation 39 (nPPF) and Equation 41 (Erf) with $\gamma_2 = \gamma_3 = 0$ against the full calculation which computes \mathcal{R} using exact forms for γ_2, γ_3 and \mathcal{F} (see Appendices of Bose et al. 2020, for all relevant expressions).

The computation of \mathcal{R} requires us to solve the evolution equations

for the spherical top-hat radius parametrised by y_h (Equation B4). This necessitates the specification of \mathcal{F} at all redshifts up to the target redshift. We then should test approximations for \mathcal{F} even at high redshifts, which is done in subsection B3, where we compare \mathcal{F} at $z = 0, 1, 4$. For comparisons of the halo model reaction, we only consider $z = 0, 1$ which are more observationally relevant.

We fit $\{q_1, q_2, q_3, q_4\}$ for the Erf model, \mathcal{F}_{Erf} . In the nPPF case, we do not fit all the 8 free parameters of $\mathcal{F}_{\text{nPPF}}$, and only consider p_1 and p_8 , treating both as constants. In principle, and indeed for unspecified theories of gravity, all 8 parameters will be fit to the data. For the comparisons made here, p_{2-7} are fixed to the theoretically predicted values quoted in section B. Fitting such a high dimensional parameter space is beyond the scope of this paper.

In what follows we fit the free parameters by performing a least square fit to the exact \mathcal{R} prediction, minimising the following merit function

$$s^2 = \sum_{j=\min}^{\max} \sum_{i=\min}^{\max} \frac{[\mathcal{R}_{\text{exact}}(k_i, z_j) - \mathcal{R}_{\text{approx}}(k_i, z_j)]^2}{\sigma_{i,j}^2}, \quad (58)$$

where we assume error bars on $\mathcal{R}_{\text{exact}}$ coming from cosmic variance and a constant systematic error added in quadrature (Zhao 2014; Blanchard et al. 2020a; Mancarella et al. 2020)

$$\sigma_{i,j}^2(k, z) = \frac{4\pi^2}{k_i^2 \Delta k_i V_{s,j}} + \sigma_{\text{sys}}^2, \quad (59)$$

where $V_{s,j} \in \{0.3, 8\} \text{ Gpc}^3/h^3$ is taken to be a stage IV survey-like volume for each bin $z_j \in \{0, 1\}$ respectively (Laureijs et al. 2011; Aghamousa et al. 2016; Mancarella et al. 2020; Blanchard et al. 2020b). We fit in the range $k_{\min} = 0.1 \leq k_i \leq 3 = k_{\max}$ which is the range over which the halo model reaction approach is roughly 2% accurate (Cataneo et al. 2019; Bose et al. 2021; Carrilho et al. 2022), sampling logarithmically, with Δk_i being the bin width. We take $\sigma_{\text{sys}} = 0.02$ to reflect the systematic error in the parametrised reaction when compared to simulations by proxy of the exact solution. The best fit parameter values are shown in Table 3.

5.1 Vainshtein example: DGP

For DGP the nPPF parameterisation reproduces the exact form of \mathcal{F} (Equation B1) for specific choices of the p_i parameters (Equation B9). On the other hand, the Erf parametrisation (Equation 41) is approximate and we fit the associated parameters. We note that DGP has no Yukawa suppression at large scales and produces a constant enhancement of the Λ CDM linear growth factor. This enhancement is controlled by the DGP degree of freedom $\Omega_{\text{rc}} \equiv 1/(4H_0^2 r_c^2)$ where r_c is the cross-over scale dictating where gravity goes from behaving

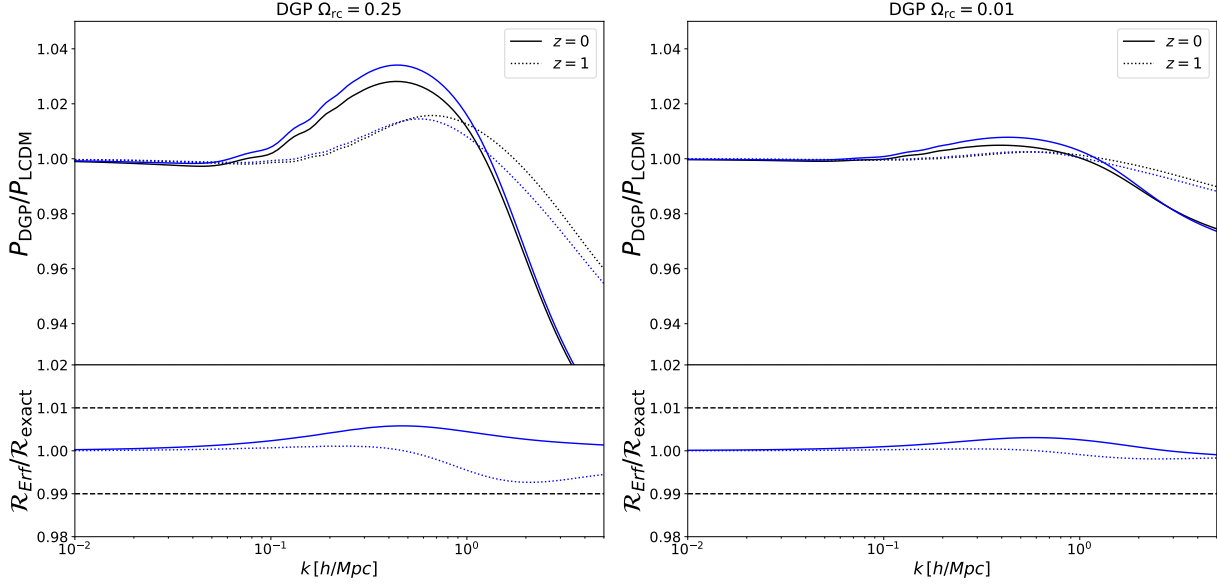


Figure 4. Top panels: The ratio of the DGP nonlinear power spectrum to the Λ CDM nonlinear power spectrum computed using halofit and the halo model reaction (see Equation 3) for the exact (black) and Erf (blue) cases. We do not show the nPPF case as it reduces to the exact solution for specific choices of its parameters. The Erf model assumes $\gamma_2 = \gamma_3 = 0$. We have normalised the ratio to unity at large scales for easier comparisons. **Bottom panels:** The ratio of halo model reactions; the Erf model R_{Erf} to the exact solution. This is equivalent to the ratio of the top panel blue to black curves. We show these results for a moderate modification, $\Omega_{\text{rc}} = 0.25$ (left) and a low modification, $\Omega_{\text{rc}} = 0.01$ (right). We plot the ratio for two observationally relevant redshifts, $z = 0$ (solid) and $z = 1$ (dotted).

Table 3. Best fit parameter values for the DGP and $f(R)$ models. The fit is performed to the exact solution for \mathcal{R} in the range $0.1 h/\text{Mpc} \leq k \leq 3 h/\text{Mpc}$ and at $z = 0, 1$ as described in the main text. For the Erf model, we do not fit q_2, q_3 and q_4 for DGP and for $f(R)$ we find the quality of fit with and without q_4 is similar. For all fits we thus set $q_4 = 0$. The nPPF is exact for DGP and so we only consider $f(R)$, fixing all p_{2-7} to the values given in Equation B10.

nPPF			Erf		
Ω_{rc}	p_1	p_8	q_1	q_2	q_3
0.25	-	-	0.76	0	0
0.01	-	-	0.71	0	0
$ f_{R0} $	p_1	p_8	q_1	q_2	q_3
10^{-5}	3	-0.8	0.9	0.35	0.65
10^{-6}	8.5	-0.5	1.65	0.7	2.45
10^{-7}	5.65	-0.45	0.6	0.8	2.15

4-dimensionally to 5-dimensionally. We consider two levels of deviation to Λ CDM: a moderate modification given by $\Omega_{\text{rc}} = 0.25$ and a small modification given by $\Omega_{\text{rc}} = 0.01$.

We only fit q_1 as we do not have any mass, environment or Yukawa-suppression scale dependence, and so we set $q_2 = q_3 = q_4 = 0$ in this case. The best fit values of q_1 are given in Table 3. Further, we employ the exact form of $\mu(a)$ in Equation 41 (see appendices of Bose et al. 2020, for the explicit expression).

In the top panels of Figure 4 we show the ratio of a DGP power spectrum to a Λ CDM spectrum with the same background expansion history, normalised to unity at linear scales for easier comparisons of nonlinear effects. The DGP spectrum is given by Equation 3. Both Λ CDM and $P_{\text{NL}}^{\text{pseudo}}$ are computed using the halofit fitting function (Takahashi et al. 2012). We see the moderate modification gives up to a 6% deviation from Λ CDM (above the linear growth enhancement)

for $k \leq 3 h/\text{Mpc}$ while the small modification can reach 2% over the same range of scales. Reassuringly, in the bottom panels we find sub-percent agreement between the Erf and exact predictions down to $k = 5 h/\text{Mpc}$, with a smaller disagreement for the smaller deviation from Λ CDM.

One can further parameterise the time dependence of q_1 which would alleviate some of these deviations, but we find these differences to be more than acceptable given the relative size compared to the modification to Λ CDM shown in the top panels. Moreover, a large number of additional degrees of freedom will be introduced in real data analyses such as intrinsic alignments and parameterisations of baryonic physics. These will be degenerate to some level with modified gravity effects (see Schneider et al. 2020, for example), allowing lower accuracy demands in the modelling of \mathcal{R} .

This additional time dependence is highlighted in Figure B1, where we find that the Erf model can match the exact form of \mathcal{F} extremely well at a fixed redshift. Upon investigation, we found this dependence to be highly degenerate with q_2 which prompted us to not introduce new freedom to the model, especially because we can achieve very good fits already, even without q_2 .

5.2 Chameleon example: Hu-Sawicki $f(R)$

For this theory we consider both the nPPF and Erf models and compare them to the exact solution (Equation B6). This model makes use of the chameleon screening mechanism which exhibits an environmental and mass dependence. It also has a Yukawa suppression which returns it to GR at large scales. The additional degree of freedom is the value of the background scalar field at $z = 0$, f_{R0} , which controls the level of deviation from GR. We consider three levels of deviation from Λ CDM, $|f_{R0}| = 10^{-5}$ (moderate modification), $|f_{R0}| = 10^{-6}$ (low modification) and $|f_{R0}| = 10^{-7}$ (very low modification). We note that the moderate $f(R)$ modification is already ruled out by

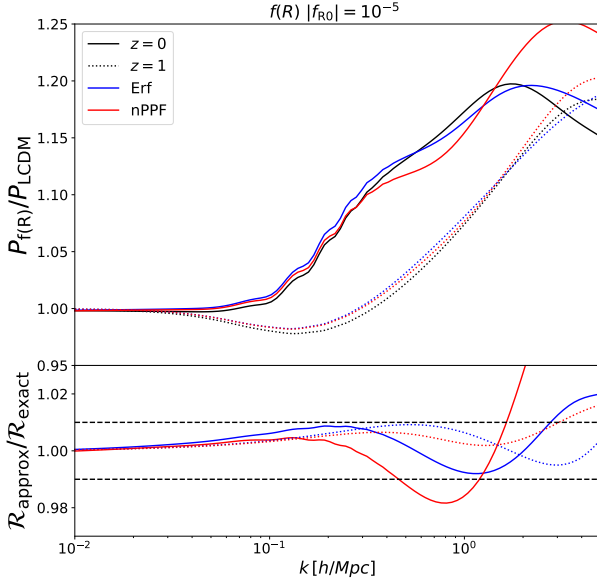


Figure 5. Top panel: The ratio of the $f(R)$ nonlinear power spectrum to the Λ CDM nonlinear power spectrum computed using halofit and the halo model reaction (see Equation 3) for the exact (black), Erf (blue) and nPPF (red) cases. **Bottom panel:** The ratio of halo model reactions; the parameterised models to the exact solution. This is equivalent to the ratio of the top panel coloured curves to the black curves. Note that both parameterised models have $\gamma_2 = \gamma_3 = 0$. We plot the ratio for two observationally relevant redshifts, $z = 0$ (solid) and $z = 1$ (dotted). We show these results for a moderate modification, $|f_{R0}| = 10^{-5}$.

data (see Cataneo et al. 2015; Desmond & Ferreira 2020; Lombriser 2014; Brax et al. 2021, for example), but provides a good flexibility test of the parameterisation.

In the nPPF case, we choose the theoretically motivated parameters given in Equation B10. These emerge from a parameterised form of $f(R)$ gravity (Lombriser et al. 2014) and so are approximate. p_1 and our new parameter p_8 remain free. Treating them both as constants, we fit them in the same way that we fit the Erf model's parameters, by minimising Equation 58. We note that the other nPPF parameters, $p_2 - p_7$, take on different forms for the chameleon screening and Yukawa suppression regimes. We only consider the screening regime which is more relevant for the spherical collapse calculation, and rely on $\mu(\hat{k}, a)$ appearing in Equation 39 to take care of the Yukawa suppression.

Yukawa suppression is relevant for large masses, large y_{env} or small values of f_{R0} . Given this, we do not expect p_8 or q_4 to be relevant for spherical collapse where $y_h \leq y_{\text{env}} \leq 1$, and even less for the 1-halo spectrum where the Sheth-Torman mass function down-weights large masses (see, for example, Schmidt et al. 2009). We verify this by performing two separate fits: the first only including the parameter sets $\{p_1\}$ and $\{q_1, q_2, q_3\}$ for the nPPF and Erf model respectively, while the second extending these sets to include p_8 and q_4 respectively.

We find that values of $q_4, p_8 \geq 0$ negligibly change the goodness of fit for the low and very low modification strengths, while sufficiently negative values degrade the fit, which is expected as the Yukawa scale begins to overlap with the screening scale. Further, we observe only a marginal improvement at $z = 0$ for $|f_{R0}| = 10^{-5}$ in the Erf case. Given this, all fits shown and quoted here set $q_4 = 0$ for the Erf case. In the nPPF case, we observe a moderate improvement for

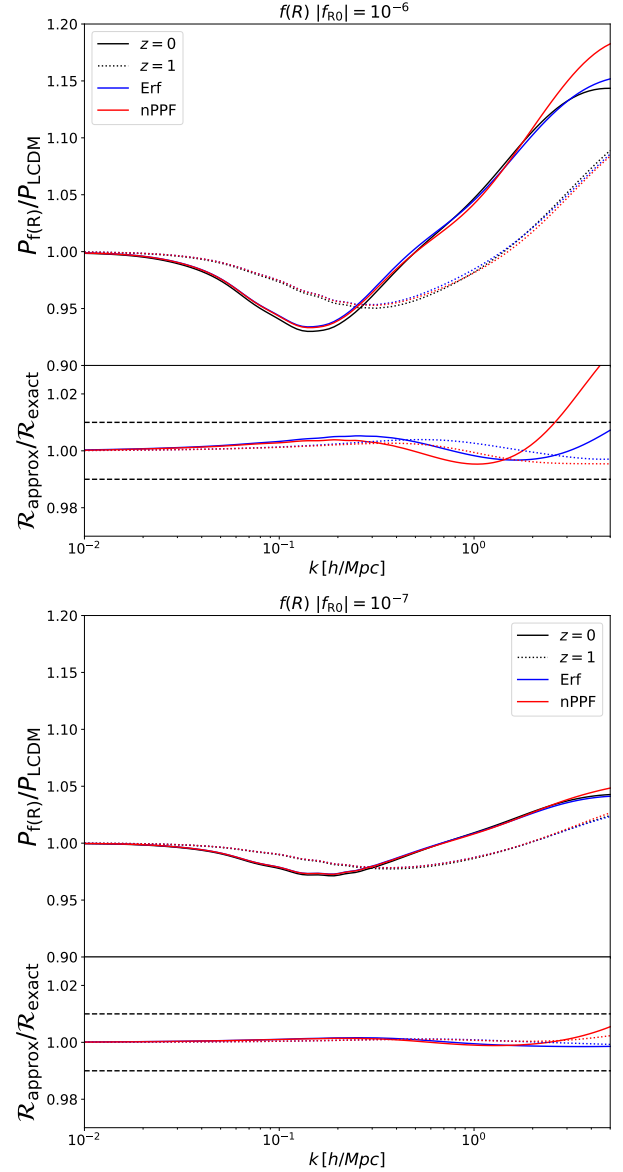


Figure 6. Same as Figure 5 for a low modification, $|f_{R0}| = 10^{-6}$ (top) and a very low modification, $|f_{R0}| = 10^{-7}$ (bottom).

$|f_{R0}| = 10^{-5}$ and so keep p_8 . We report the best-fit parameters in Table 3.

The $f(R)$ results are shown in Figure 5 and Figure 6. We see the moderate modification can reach a 20% deviation from Λ CDM for $k \leq 3h/\text{Mpc}$ while the low and very low modifications reach 10% and 3% respectively. Both parameterisations do well in modelling the moderate modification case $|f_{R0}| = 10^{-5}$, shown in Figure 5. The Erf model prediction for \mathcal{R} stays within 1% of the exact solution for $k \leq 3h/\text{Mpc}$. Similarly, the nPPF remains within 2% for $k \leq 2h/\text{Mpc}$. The situation improves for the lower modification cases, shown in Figure 5. These comparisons exhibit sub-1% agreement between the Erf (nPPF) model and exact solution for $k \leq 5(3) h/\text{Mpc}$ at $z = 0$ and $z = 1$.

This indicates that for the Erf model, degeneracies between q_{1-3} and q_4 make the latter parameter unnecessary. We note that the fit of q_{1-3} becomes insensitive to the value of q_4 if it is sufficiently large, here found to be $q_4 = 0$. For the nPPF model, the additional freedom

provided by p_8 is necessary to improve the fit, but it does not help substantially for observationally viable values of f_{R0} . Further, we remind the reader that we do not know p_{2-7} a priori for unspecified theories of gravity, and so the importance of p_8 is likely to be minimal when considering these additional degrees of freedom.

Lastly, we remark that the Erf model gives a good fit for a range of values for q_{1-3} ¹⁰. The values quoted in Table 3 are only the best fit values, which are also very dependent on Equation 59. This makes it hard to extract any further dependence on f_{R0} in Equation 41 (note this already depends on $\mu(k, a)$), which is also beyond the scope of this parametrisation which aims to be general in terms of gravitational degrees of freedom.

6 SUMMARY

In this paper we have presented a significant extension of the code described in Bose et al. (2020) which produces nonlinear corrections to the matter power spectrum coming from beyond- Λ CDM physics in the form of the halo model reaction \mathcal{R} . In particular, we have focused on implementing parameterisations of key equations, in particular the background expansion history and the linear and nonlinear Poisson equations.

For the linear scales and background we have considered the effective field theory of dark energy (EFTofDE) while for the nonlinear scales we have considered two distinct parameterisations, a nonlinear parameterised post-Friedmannian (nPPF) based model and a more phenomenological model based on the error function (Erf). Together, these give a general parameterisation of the nonlinear matter power spectrum in Horndeski models. We neglect loop corrections in these parameterisations but leave these as viable additions and we provide theoretical and numerical means of deriving these for the Horndeski class of theories. This being said, we remark that the nonlinear parameterisations are completely general, and so to move beyond the Horndeski class it is sufficient to parametrise only the background expansion history and the linear modification to the Poisson equation. Further, the nonlinear parameterisations also have unscreened limits, and so we are not restricted to theories exhibiting screening. In summary, this work presents a fast, accurate and highly general nonlinear power spectrum predictor for non-standard models of gravity and cosmology including massive neutrinos, parameterised with a minimal set of free, physically meaningful constants.

We have tested these parameterisations against the full solutions for \mathcal{R} in two beyond- Λ CDM models, Hu-Sawicki $f(R)$ and DGP gravity. This has identified a minimal set of 3 free functions of time and 3 dimensionless, positive, $\mathcal{O}(1)$ dimensionless constants, which can replicate the exact solutions to within 1% at $k \leq 5h/\text{Mpc}$ and at $z \leq 1$ for modifications to GR within current data constraints and within the Horndeski class. This level of imprecision is sub-dominant to the 2% accuracy currently achieved by the reaction method at these scales (Cataneo et al. 2019, 2020; Bose et al. 2021; Carrilho et al. 2022). We suspect that this minimal parametrisation is acceptable for upcoming Stage IV cosmic shear analyses given the flexibility of the nonlinear parameterisation and the many other nuisance degrees of freedom entering a real data analyses, such as those characterising baryonic physics or intrinsic galaxy alignments (see, for example, Tröster et al. 2021).

The Erf model is also highly model independent, capturing the

¹⁰ Similar fits were found for $\mathcal{O}(0.1)$ values for these parameters.

basic phenomenology of screening mechanisms. It can thus be suitable for analyses targeting general deviations from Λ CDM. For example, one may perform a model independent analysis combining the Erf parametrisation with the linear theory growth index γ -parametrisation (Peebles 1980; Linder & Cahn 2007) (also see Eq. 47 of Kennedy et al. 2018) and say the background parametrisation of Chevallier & Polarski (2001); Linder (2003), giving 6 free constants characterising general deviations from Λ CDM in the matter power spectrum at a wide range of scales. On the other hand, the nPPF approach is complementary as it can be directly related to specific actions of Nature, making it very suitable when we look to constrain more specific classes of theories.

In future work we will test the robustness of the minimal parameterisation, and forecast constraints on deviations to Λ CDM by performing full Markov chain Monte Carlo (MCMC) analyses on mock data of the cosmic shear spectrum. Consistency and accuracy checks can also be performed using recently developed parametrised modified gravity simulations (Hassani & Lombriser 2020; Srinivasan et al. 2021; Wright et al. 2022). On this note, our code is as fast as the original ReACT and so is capable of running MCMC analyses. Despite its appreciable baseline speed, we aim to make this even faster by creating emulators based off halo model reaction predictions using the recently released CosmoPower code (Spurio Mancini et al. 2022) which will highly optimise such analyses. It is a future plan to also perform real data analyses on currently available cosmic shear data to constrain deviations to Λ CDM using the general minimal parametrisation given in Table 2.

It is currently an ongoing project to also extend the halo model reaction to redshift space and biased tracers in a vein similar to Bose et al. (2019). We also plan to include interacting dark energy parametrisations (Gleyzes et al. 2015; Skordis et al. 2015), a scenario where essentially one decouples the baryons from Λ CDM modifications, contrary to the scenario considered in this paper where all matter is coupled to the scalar field.

ACKNOWLEDGMENTS

The authors would like to thank Matteo Cataneo and Daniel B Thomas for useful comments and suggestions. BB, JK and LL acknowledge support from the Swiss National Science Foundation (SNSF) Professorship grant Nos. 170547 & 202671. BB was supported by a UK Research and Innovation Stephen Hawking Fellowship (EP/W005654/1). ANT acknowledges support from a STFC Consolidated Grant. MT's research is supported by a doctoral studentship in the School of Physics and Astronomy, University of Edinburgh. AP is a UK Research and Innovation Future Leaders Fellow [grant MR/S016066/1]. For the purpose of open access, the author has applied a Creative Commons Attribution (CC BY) licence to any Author Accepted Manuscript version arising from this submission.

DATA AVAILABILITY

The software used in this article is publicly available in the ACTio-ReACTio repository at <https://github.com/nebblu/ACTio-ReACTio>. In the same repository we also provide two Mathematica notebooks: `GtoPT.nb` that explicitly calculates the modified gravity 1st, 2nd and 3rd order Poisson equation modifications for particular covariant theories of gravity as well as provides maps between the EFTofDE M - and α -bases, and `Nonlinear.nb`

which provides expressions, tests and comparisons of the nonlinear Poisson equation modifications.

REFERENCES

Abazajian K. N., et al., 2016, CMB-S4 Science Book, First Edition ([arXiv:1610.02743](https://arxiv.org/abs/1610.02743))

Abbott B. P., et al., 2017, *Astrophys. J.*, 848, L13

Adams A., Arkani-Hamed N., Dubovsky S., Nicolis A., Rattazzi R., 2006, *JHEP*, 10, 014

Agarwal S., Feldman H. A., 2011, *Mon. Not. Roy. Astron. Soc.*, 410, 1647

Aghamousa A., et al., 2016, The DESI Experiment Part I: Science, Targeting, and Survey Design ([arXiv:1611.00036](https://arxiv.org/abs/1611.00036))

Aghanim N., et al., 2020, *Astron. Astrophys.*, 641, A6

Alam S., et al., 2021, *Phys. Rev. D*, 103, 083533

Angulo R. E., Zennaro M., Contreras S., Aricò G., Pellejero-Ibañez M., Stücker J., 2021, *MNRAS*, 507, 5869

Appleby S., Linder E. V., 2020, *JCAP*, 12, 036

Aricò G., Angulo R. E., Zennaro M., 2021, [doi:10.12688/openresearcheurope.143102](https://doi.org/10.12688/openresearcheurope.143102)

Arnold C., Li B., Giblin B., Harnois-Déraps J., Cai Y.-C., 2021, FORGE – the f(R) gravity cosmic emulator project I: Introduction and matter power spectrum emulator ([arXiv:2109.04984](https://arxiv.org/abs/2109.04984))

Babichev E., Mukhanov V., Vikman A., 2008, *JHEP*, 02, 101

Babichev E., Deffayet C., Ziour R., 2009, *Int. J. Mod. Phys. D*, 18, 2147

Baker T., Bellini E., Ferreira P. G., Lagos M., Noller J., Sawicki I., 2017, *Phys. Rev. Lett.*, 119, 251301

Baker T., et al., 2022, *JCAP*, 08, 031

Battye R. A., Pace F., Trinh D., 2018, *Phys. Rev.*, D98, 023504

Bellini E., Sawicki I., 2014, *JCAP*, 07, 050

Bellini E., Cuesta A. J., Jimenez R., Verde L., 2016, *J. Cosmology Astropart. Phys.*, 2016, 053

Bernardeau F., Colombi S., Gaztanaga E., Scoccimarro R., 2002, *Phys. Rept.*, 367, 1

Blanchard A., et al., 2020a, *Astron. Astrophys.*, 642, A191

Blanchard A., et al., 2020b, *Astron. Astrophys.*, 642, A191

Bloomfield J. K., Flanagan E. E., Park M., Watson S., 2013, *JCAP*, 1308, 010

Bose B., Koyama K., 2016, *JCAP*, 1608, 032

Bose B., Winther H. A., Pourtsidou A., Casas S., Lombriser L., Xia Q., Cataneo M., 2019, *JCAP*

Bose B., Cataneo M., Tröster T., Xia Q., Heymans C., Lombriser L., 2020, *Mon. Not. Roy. Astron. Soc.*, 498, 4650

Bose B., et al., 2021, *Mon. Not. Roy. Astron. Soc.*, 508, 2479

Brax P., Valageas P., 2013, *Phys. Rev. D*, 88, 023527

Brax P., Valageas P., 2014, *Phys. Rev. D*, 90, 023508

Brax P., Casas S., Desmond H., Elder B., 2021, *Universe*, 8, 11

Burgess C. P., 2004, *Annals Phys.*, 313, 283

Burrage C., Sakstein J., 2018, *Living Rev. Rel.*, 21, 1

Burrage C., de Rham C., Heisenberg L., Tolley A. J., 2012, *JCAP*, 07, 004

Carrilho P., Carrion K., Bose B., Pourtsidou A., Hidalgo J. C., Lombriser L., Baldi M., 2022, *Mon. Not. Roy. Astron. Soc.*, 512, 3691

Cataneo M., et al., 2015, *Phys. Rev. D*, 92, 044009

Cataneo M., Lombriser L., Heymans C., Mead A., Barreira A., Bose S., Li B., 2019, *Mon. Not. Roy. Astron. Soc.*, 488, 2121

Cataneo M., Emberson J., Inman D., Harnois-Déraps J., Heymans C., 2020, *Mon. Not. Roy. Astron. Soc.*, 491, 3101

Charmousis C., Copeland E. J., Padilla A., Saffin P. M., 2012, *Phys. Rev. Lett.*, 108, 051101

Chevallier M., Polarski D., 2001, *Int. J. Mod. Phys.*, D10, 213

Cooray A., Sheth R. K., 2002, *Phys. Rept.*, 372, 1

Creminelli P., Vernizzi F., 2017, *Phys. Rev. Lett.*, 119, 251302

Creminelli P., Lewandowski M., Tambalo G., Vernizzi F., 2018, *JCAP*, 1812, 025

Creminelli P., Tambalo G., Vernizzi F., Yingcharoenrat V., 2020, *J. Cosmology Astropart. Phys.*, 2020, 002

Cusin G., Lewandowski M., Vernizzi F., 2018a, *JCAP*, 04, 005

Cusin G., Lewandowski M., Vernizzi F., 2018b, *JCAP*, 04, 061

De Felice A., Tsujikawa S., 2012, *JCAP*, 1202, 007

Deffayet C., Pujolas O., Sawicki I., Vikman A., 2010, *JCAP*, 10, 026

Desmond H., Ferreira P. G., 2020, *Phys. Rev. D*, 102, 104060

Dvali G., Gabadadze G., Porrati M., 2000, *Phys. Lett.*, B485, 208

Euclid Collaboration et al., 2020, arXiv e-prints, p. [arXiv:2010.11288](https://arxiv.org/abs/2010.11288)

Ezquiaga J. M., Zumalacárregui M., 2017, *Phys. Rev. Lett.*, 119, 251304

Fernandes P. G. S., Carrilho P., Clifton T., Mulryne D. J., 2022, *Class. Quant. Grav.*, 39, 063001

Frusciante N., Peronon L., 2020, *Phys. Rept.*, 857, 1

Frusciante N., Papadomanolakis G., Silvestri A., 2016, *JCAP*, 07, 018

Frusciante N., Peirone S., Casas S., Lima N. A., 2019, *Phys. Rev. D*, 99, 063538

Giblin B., Cataneo M., Moews B., Heymans C., 2019, *Mon. Not. Roy. Astron. Soc.*, 490, 4826

Gleyzes J., Langlois D., Mancarella M., Vernizzi F., 2015, *JCAP*, 08, 054

Gspone R., Noller J., 2022, *Phys. Rev. D*, 105, 064002

Gubitosi G., Piazza F., Vernizzi F., 2013, *JCAP*, 1302, 032

Hassani F., Lombriser L., 2020, *Mon. Not. Roy. Astron. Soc.*, 497, 1885

Hernández-Aguayo C., Ruan C.-Z., Li B., Arnold C., Baugh C. M., Klypin A., Prada F., 2022, *JCAP*, 01, 048

Hinterbichler K., Khoury J., 2010, *Phys. Rev. Lett.*, 104, 231301

Horndeski G. W., 1974, *Int. J. Theor. Phys.*, 10, 363

Hu W., Sawicki I., 2007, *Phys. Rev.*, D76, 064004

Hu B., Raveri M., Frusciante N., Silvestri A., 2014, *Phys. Rev.*, D89, 103530

Huang Z., 2016, *Phys. Rev. D*, 93, 043538

Ivezic v., et al., 2019, *Astrophys. J.*, 873, 111

Joudaki S., Ferreira P. G., Lima N. A., Winther H. A., 2022, *Phys. Rev. D*, 105, 043522

Kennedy J., Lombriser L., Taylor A., 2017, *Phys. Rev.*, D96, 084051

Kennedy J., Lombriser L., Taylor A., 2018, *Phys. Rev.*, D98, 044051

Khan A., Taylor A., 2022, A minimal self tuning model to solve the cosmological constant problem ([arXiv:2201.09016](https://arxiv.org/abs/2201.09016))

Khoury J., Weltman A., 2004, *Phys. Rev. Lett.*, 93, 171104

Koyama K., 2018, *Int. J. Mod. Phys.*, D27, 1848001

Laureijs R., et al., 2011,

Lewis A., Challinor A., Lasenby A., 2000, *Astrophys. J.*, 538, 473

Li B., Efstathiou G., 2012, *Mon. Not. Roy. Astron. Soc.*, 421, 1431

Linder E. V., 2003, *Phys. Rev. Lett.*, 90, 091301

Linder E. V., Cahn R. N., 2007, *Astropart. Phys.*, 28, 481

Lombriser L., 2014, *Annalen Phys.*, 526, 259

Lombriser L., 2016, *JCAP*, 11, 039

Lombriser L., Lima N. A., 2017, *Phys. Lett.*, B765, 382

Lombriser L., Taylor A., 2015a, *JCAP*, 11, 040

Lombriser L., Taylor A., 2015b, *Phys. Rev. Lett.*, 114, 031101

Lombriser L., Taylor A., 2016, *JCAP*, 1603, 031

Lombriser L., Koyama K., Li B., 2014, *JCAP*, 03, 021

Lombriser L., Dalang C., Kennedy J., Taylor A., 2019, *JCAP*, 01, 041

Mancarella M., Kennedy J., Bose B., Lombriser L., 2020, arXiv e-prints, p. [arXiv:2012.03992](https://arxiv.org/abs/2012.03992)

Martin J., 2012, *Comptes Rendus Physique*, 13, 566

McManus R., Lombriser L., Peñarrubia J., 2016, *JCAP*, 11, 006

Mead A., Peacock J., Heymans C., Joudaki S., Heavens A., 2015, *Mon. Not. Roy. Astron. Soc.*, 454, 1958

Mead A., Heymans C., Lombriser L., Peacock J., Steele O., Winther H., 2016, *Mon. Not. Roy. Astron. Soc.*, 459, 1468

Mead A. J., Brieden S., Tröster T., Heymans C., 2021, *MNRAS*, 502, 1401

Melville S., Noller J., 2020, *Phys. Rev. D*, 101, 021502

Noller J., 2020, *Phys. Rev. D*, 101, 063524

Noller J., Nicola A., 2019a, *Phys. Rev. D*, 99, 103502

Noller J., Nicola A., 2019b, *Phys. Rev. D*, 99, 103502

Pace F., Battye R., Bellini E., Lombriser L., Vernizzi F., Bolliet B., 2021, *JCAP*, 06, 017

Padilla A., 2015, Lectures on the Cosmological Constant Problem

Peebles P. J. E., 1980, The large-scale structure of the universe. Research supported by the National Science Foundation. Princeton, N.J., Princeton University Press, 1980. 435 p.

Peirone S., Koyama K., Pogosian L., Raveri M., Silvestri A., 2018, *Phys. Rev. D*, 97, 043519

Perlmutter S., et al., 1999, *Astrophys. J.*, 517, 565
 Pogosian L., Silvestri A., 2016, *Phys. Rev. D*, 94, 104014
 Puchwein E., Baldi M., Springel V., 2013, *Mon. Not. Roy. Astron. Soc.*, 436, 348
 Raveri M., Hu B., Frusciante N., Silvestri A., 2014, *Phys. Rev.*, D90, 043513
 Reall H. S., 2021, *Phys. Rev. D*, 103, 084027
 Remevey C., Kennedy J., Lombriser L., 2020, *JCAP*, 12, 032
 Riess A. G., et al., 1998, *Astron. J.*, 116, 1009
 Sakstein J., Jain B., 2017, *Phys. Rev. Lett.*, 119, 251303
 Sawicki I., Bellini E., 2015, *Phys. Rev. D*, 92, 084061
 Schmidt F., 2010, *Phys. Rev.*, D81, 103002
 Schmidt F., Lima M. V., Oyaizu H., Hu W., 2009, *Phys. Rev.*, D79, 083518
 Schmidt F., Hu W., Lima M., 2010, *Phys. Rev.*, D81, 063005
 Schneider A., et al., 2020, *JCAP*, 04, 020
 Silvestri A., Pogosian L., Buniy R. V., 2013, *Phys. Rev. D*, 87, 104015
 Skordis C., Poutsidou A., Copeland E. J., 2015, *Phys. Rev.*, D91, 083537
 Sobral Blanco D., Lombriser L., 2020, *Phys. Rev. D*, 102, 043506
 Spurio Mancini A., et al., 2019, *Mon. Not. Roy. Astron. Soc.*, 490, 2155
 Spurio Mancini A., Piras D., Alsing J., Joachimi B., Hobson M. P., 2022, *Mon. Not. Roy. Astron. Soc.*, 511, 1771
 Srinivasan S., Thomas D. B., Pace F., Battye R., 2021, arXiv e-prints, [p. arXiv:2103.05051](https://arxiv.org/abs/2103.05051)
 Taddei L., Catena R., Pietroni M., 2014, *Phys. Rev. D*, 89, 023523
 Takahashi R., Sato M., Nishimichi T., Taruya A., Oguri M., 2012, *Astrophys. J.*, 761, 152
 Takushima Y., Terukina A., Yamamoto K., 2015, *Phys. Rev.*, D92, 104033
 Thomas D. B., Clifton T., Anton T., 2022, Scale-Dependent Gravitational Couplings in Parameterised Post-Newtonian Cosmology ([arXiv:2207.14713](https://arxiv.org/abs/2207.14713))
 Traykova D., Bellini E., Ferreira P. G., 2019, *JCAP*, 08, 035
 Tröster T., et al., 2021, *Astron. Astrophys.*, 649, A88
 Vainshtein A., 1972, *Phys. Lett.*, B39, 393
 Weinberg S., 1989, *Rev. Mod. Phys.*, 61, 1
 Will C. M., 1993, Theory and Experiment in Gravitational Physics
 Will C. M., 2014, *Living Rev. Rel.*, 17, 4
 Winther H. A., Koyama K., Manera M., Wright B. S., Zhao G.-B., 2017, *JCAP*, 08, 006
 Wright B. S., Gupta A. S., Baker T., Valogiannis G., 2022, Hi-COLA: Fast, approximate simulations of structure formation in Horndeski gravity ([arXiv:2209.01666](https://arxiv.org/abs/2209.01666))
 Zhao G.-B., 2014, *Astrophys. J. Suppl.*, 211, 23
 de Felice A., Kobayashi T., Tsujikawa S., 2011, *Physics Letters B*, 706, 123
 de Rham C., Melville S., 2018, *Phys. Rev. Lett.*, 121, 221101
 de Rham C., Tolley A. J., 2020, *Phys. Rev. D*, 102, 084048
 de Rham C., Melville S., Noller J., 2021, *JCAP*, 08, 018

APPENDIX A: LINEAR POISSON MODIFICATIONS

A1 Horndeski in the α -basis

The linear modification to the Poisson equation in the Horndeski class of EFTofDE, under the quasi-static approximation, and in the α -basis, $\{H, \alpha_M, \alpha_B, \alpha_K, \alpha_T\}$, is given by

$$\mu(k, a) = \frac{2}{\kappa^2} \frac{f_1(a) + f_2(a)a^2/k^2}{f_3(a) + f_4(a)a^2/k^2}, \quad (\text{A1})$$

where the constituent functions are given by

$$f_1 = B_2 C_3 - C_1 B_3, \quad (\text{A2})$$

$$f_2 = B_2 C_\pi, \quad (\text{A3})$$

$$\begin{aligned} f_3 = & A_1 [B_3 C_2 - B_1 C_3(k, a)] \\ & + A_2 [B_1 C_1 - B_2 C_2] \\ & + A_3 [B_2 C_3 - B_3 C_1], \end{aligned} \quad (\text{A4})$$

$$f_4 = [A_3 B_2 - A_1 B_1] C_\pi. \quad (\text{A5})$$

Finally, we give the A , B and C functions in terms of the α -basis as (Pogosian & Silvestri 2016)

$$A_1 = 2M^2, \quad (\text{A6})$$

$$A_2 = \alpha_B H M^2, \quad (\text{A7})$$

$$A_3 = 0, \quad (\text{A8})$$

$$B_1 = -\frac{1}{c_T^2}, \quad (\text{A9})$$

$$B_2 = 1, \quad (\text{A10})$$

$$B_3 = \frac{(-\alpha_M + \alpha_T)H}{c_T^2}, \quad (\text{A11})$$

$$C_1 = -B_3 M^2 c_T^2, \quad (\text{A12})$$

$$C_2 = \frac{A_2}{2}, \quad (\text{A13})$$

$$\begin{aligned} C_3 = & c + \frac{HM^2}{2} \left[-2\alpha_T H + \alpha_M^2 c_T^2 H + aH\alpha'_B + aH\alpha'_M \right. \\ & \left. + a\alpha_T H\alpha'_M + 2a\alpha_T H' + a^2\alpha'_T H' + \alpha_B [(1 + \alpha_M)H + aH'] \right. \\ & \left. + a\alpha_M [H(1 - \alpha_T + 2a\alpha'_T) + ac_T^2 H'] + a^2 H\alpha''_T \right], \end{aligned} \quad (\text{A14})$$

$$\begin{aligned} C_\pi = & -\frac{1}{4} aH \left[12cH' + HM^2(6\alpha_M^2 c_T^2 HH' \right. \\ & \left. + 6\alpha_B(2a(H')^2 + H[(4 + \alpha_M)H' + aH'']) \right. \\ & \left. + \alpha_M(c_T^2(12a(H')^2 - \bar{R}') + 6H(2(2c_T^2 + a\alpha'_T)H' + ac_T^2 H'')) \right. \\ & \left. + a[12(\alpha_T + a\alpha'_T)(H')^2 \right. \\ & \left. - \alpha'_T \bar{R}' + 6H(H'(\alpha'_B + c_T^2 \alpha'_M + 5\alpha'_T + a\alpha''_T) + a\alpha'_T H'')] \right], \end{aligned} \quad (\text{A15})$$

where $c_T^2 = (1 + \alpha_T)$ and \bar{R} is the background Ricci scalar. The $c(a)$ parameter (Equation 22) in the α -basis is given by

$$\begin{aligned} c(a) = & -M^2 \left[\frac{3H_0^2 \Omega_{m,0}}{2a^3 \kappa^2 M^2} \right. \\ & + \frac{1}{2} H \left(aH' [(2 + \alpha_M)c_T^2 + a\alpha'_T] \right. \\ & \left. + H(c_T^2 [(\alpha_M - 1)\alpha_M + a\alpha'_M] + 2a\alpha_M \alpha'_T + a^2 \alpha''_T) \right], \end{aligned} \quad (\text{A16})$$

where we have used $\rho_m = 3H_0^2 \Omega_{m,0}/(\kappa^2 a^3)$, with $\Omega_{m,0}$ being the matter density fraction today and $H_0 = H(a = 1)$ is the Hubble constant.

We note that in our code we make the redefinition $M^2 \kappa^2 = M^2/m_0^2 \rightarrow M^2$ where m_0^2 is the Planck mass. Further, we comment on the flexibility offered here. One can choose to specify any two of $\{\alpha_M, M^2, H\}$. If H is specified then either α_M or M^2 must also be specified, with the third function given by the relation in Equation 25. If H is not specified, then we must solve the Friedmann equations to obtain H . As a default in our code, H is specified and it is assumed that the specified expressions for α_M and M^2 are consistent with Equation 25.

We can also take the small scale ($k \rightarrow \infty$) limit of Equation A1 to get a simpler expression valid at scales where the QS is a safer approximation and for models exhibiting negligible scale dependence in the linear growth. This is given by

$$\mu_\infty = \frac{1}{M^2 \kappa^2} (1 + \alpha_T + \beta_\xi), \quad (\text{A17})$$

where

$$\beta_\xi = \frac{2}{c_s^2 \alpha} \left(c_T^2 \frac{\alpha_B}{2} + \alpha_M - \alpha_T \right)^2 \quad (\text{A18})$$

with c_s^2 and α and α given by [Equation 29](#) and [Equation 30](#).

A2 Example: Hu-Sawicki $f(R)$

In this section we derive the relevant EFTofDE parameters and linear Poisson modification for the Hu-Sawicki form of $f(R)$ gravity ([Hu & Sawicki 2007](#)). This exercise is also performed in the `GtoPT` notebook provided in the `ACTio-ReACTio` github repository.

The action in $f(R)$ gravity is given by

$$\begin{aligned} S &= \int d^4x \sqrt{-g} \frac{1}{2\kappa^2} (R + f(R)) \\ &\approx \int d^4x \sqrt{-g} \frac{1}{2\kappa^2} (R + f(\bar{R}) + f_R(\bar{R})(R - \bar{R})) \\ &= \int d^4x \sqrt{-g} \frac{1}{2\kappa^2} ((1 + f_R)R + f - f_R\bar{R}), \end{aligned} \quad (\text{A19})$$

where $f_R = df(R)/dR$ and we have performed a Taylor expansion in the second line. We can then map this action onto the functions given in [Equation 2](#) together with an identification of the scalar degree of freedom $\phi \equiv (1 + f_R)/\kappa^2$ ([de Felice et al. 2011](#)):

$$G_2 = -\frac{1}{2\kappa^2}(\bar{R}f_R - f), \quad G_3 = 0, \quad \text{and} \quad G_4 = \frac{1}{2\kappa^2}(1 + f_R). \quad (\text{A20})$$

If we now write down the action in the ADM formalism and use the Gauss-Codazzi relation, we can compare to [Equation 18](#) and [Equation 19](#) to get

$$\Omega = (1 + f_R), \quad \Lambda = \frac{1}{2\kappa^2}(f - \bar{R}f_R), \quad c = \bar{M}_2^2 = \bar{M}_1^3 = M_2^4 = 0. \quad (\text{A21})$$

Using [Equation 25](#) - [Equation 27](#) we have

$$\alpha_M = \frac{af'_R}{1 + f_R}, \quad (\text{A22})$$

$$\alpha_T = 0, \quad (\text{A23})$$

$$\alpha_B = -\frac{af'_R}{1 + f_R}, \quad (\text{A24})$$

$$\alpha_K = 0, \quad (\text{A25})$$

with

$$M^2 = \frac{(1 + f_R)}{\kappa^2}, \quad (\text{A26})$$

where a prime denotes a scale factor derivative. When substituting into the expressions in [Appendix A1](#) we get the following solution for μ ([Equation A1](#))

$$\mu = \frac{1}{1 + f_R} \left[1 + \left(\frac{k}{a} \right)^2 \frac{1}{3\tilde{\Pi}(k, a)} \right], \quad (\text{A27})$$

where

$$\tilde{\Pi}(k, a) = \left(\frac{k}{a} \right)^2 + (1 + f_R) \frac{\bar{R}_f}{3}, \quad (\text{A28})$$

and

$$\bar{R}_f \equiv \frac{d\bar{R}}{df_R} = f_{RR}^{-1} \left(\frac{\bar{R}'}{f'_R} \right). \quad (\text{A29})$$

In the Hu-Sawicki model we have the following choice for $f(R)$

$$f(R) = -m^2 \frac{c_1(R/m^2)^n}{c_2(R/m^2)^n + 1}, \quad (\text{A30})$$

where in this work we set the index $n = 1$ and the mass scale m^2 , c_1 and c_2 are free parameters to be constrained by data. Taking the derivative of [Equation A30](#) with respect to R and the high curvature limit ($R \gg m^2$) gives

$$f_R = -\frac{c_1}{c_2^2} \left(\frac{m^2}{R} \right)^2. \quad (\text{A31})$$

By rearranging this equation and evaluating at the background level at $a = 1$ (today), we can apply the following standard reparameterisation

$$\frac{c_1}{c_2^2} = -\bar{f}_{R0} \left(\frac{\bar{R}_0}{m^2} \right)^2, \quad (\text{A32})$$

where \bar{f}_{R0} is the background value of f_R evaluated today and is a free parameter governing the level of modification to Λ CDM at the level of structure formation. Substituting [Equation A32](#) into [Equation A31](#) gives

$$f_R = \bar{f}_{R0} \left(\frac{\bar{R}_0}{R} \right)^2. \quad (\text{A33})$$

Further, we have

$$f_{RR} = -2\bar{f}_{R0} \left(\frac{\bar{R}_0}{R} \right)^2 \frac{1}{R}. \quad (\text{A34})$$

Using the background expression for f_{RR} in [Equation A29](#) and substituting into [Equation A28](#) gives

$$\tilde{\Pi}(k, a) = \left(\frac{k}{a} \right)^2 + (1 + f_R) \frac{1}{6|f_{R0}|} \frac{\bar{R}^3}{\bar{R}_0^2}. \quad (\text{A35})$$

Now if we approximate the background to be close to Λ CDM, as supported by observations and by construction for $|f_{R0}| \ll 1$, we have

$$\bar{R} \approx 3 \frac{H_0^2}{a^3} \left(\Omega_{m,0} + 4a^3 \Omega_{\Lambda,0} \right), \quad (\text{A36})$$

where $\Omega_{\Lambda,0} = 1 - \Omega_{m,0}$ for a flat Λ CDM universe. Taking $a = 1$ we have the curvature today

$$\bar{R}_0 \approx 3H_0^2 \left(4 - 3\Omega_{m,0} \right). \quad (\text{A37})$$

Finally substituting \bar{R} and \bar{R}_0 in [Equation A35](#) we get the expression for μ as it appears in `ACTio-ReACTio` ([Bose et al. 2020](#))

$$\mu = 1 + \left(\frac{k}{a} \right)^2 \frac{1}{3\tilde{\Pi}(k, a)}, \quad (\text{A38})$$

with

$$\tilde{\Pi}(k, a) = \left(\frac{k}{a} \right)^2 + \frac{\Xi(a)^3}{2f_0(4 - 3\Omega_{m,0})^2}, \quad (\text{A39})$$

$$\Xi(a) = \frac{\Omega_{m,0} + 4a^3 \Omega_{\Lambda,0}}{a^3}, \quad (\text{A40})$$

where $f_0 = |f_{R0}|/H_0^2$.

We make the crucial note here that in the derivation above we have over-constrained our system. Namely we have specified all of Ω , c as well as set $H = H_{\Lambda\text{CDM}}$. If we use [Equation A22](#)-[Equation A26](#) together with $H = H_{\Lambda\text{CDM}}$ we find that $c \neq 0$ and we don't recover [Equation A38](#). This follows directly from the fact that $H_{\Lambda\text{CDM}}$ is

not an exact solution for the Friedmann equations in $f(R)$ which implicitly assumes $c = 0$.

In our code we give the option to over constrain by specifying $c(a)$. Alternatively, one can code in the Friedmann equations and solve for $H(a)$. This of course increases computational inefficiency. To partially alleviate this issue, we can also place the additional constraint on $c_s^2(a)$ instead of c which has well motivated physical priors (see text around [Equation 29](#)). The relationship between $c_s^2(a)$ and $c(a)$ is derived from [Equation 29](#) and [Equation A16](#). It is given explicitly in the GtoPT notebook as well as the **Actio-Reactio** source code.

The derivation of the 2nd and 3rd order modifications to the Poisson equation (see [Equation 14](#)) from the ADM decomposed action requires us to go to higher order in the metric perturbations. We do not do this here as we omit these corrections from our code due to computational difficulty and the low level of impact they have on the final nonlinear power spectrum (see Section 5). However, in the provided Mathematica notebook, GtoPT, one can go from a specified G_i of the Horndeski Lagrangian to μ , γ_2 and γ_3 following the map given in [Bose & Koyama \(2016\)](#). We provide a number of examples in that notebook and refer the reader to [Bose et al. \(2020\)](#); [Bose & Koyama \(2016\)](#) for the forms of μ , γ_2 and γ_3 in DGP and Hu-Sawicki $f(R)$ gravity.

APPENDIX B: NONLINEAR POISSON MODIFICATIONS

B1 Exact forms

We provide the exact forms for the nonlinear modification to the Poisson equation (see [Equation 13](#)) in DGP and $f(R)$ gravity, which are reproduced from [Bose et al. \(2020\)](#).

The modification in DGP is given by ([Schmidt et al. 2010](#))

$$\mathcal{F}_{\text{DGP}} = \frac{2}{3\beta(a)} \frac{\sqrt{1+s^3}-1}{s^3}, \quad (\text{B1})$$

where¹¹

$$s = \left[\frac{2\Omega_{m,0}(\delta+1)}{9a^3\beta(a)^2\Omega_{rc}} \right]^{\frac{1}{3}}, \quad (\text{B2})$$

δ being the nonlinear over-density given by

$$\delta = y^{-3}(1+\delta_i) - 1, \quad (\text{B3})$$

with δ_i being the initial over-density and

$$y \equiv \frac{R_{\text{TH}}/a}{R_i/a_i}, \quad (\text{B4})$$

R_{TH} and R_i being the physical halo top-hat radius at the target scale factor a and the initial scale factor a_i respectively. $\Omega_{rc} \equiv 1/(4H_0^2 r_c^2)$ where r_c is the cross-over scale and is the free parameter of the theory governing the level of modification. Finally, $\beta(a)$ is given by

$$\beta(a) \equiv 1 + \frac{H}{H_0} \frac{1}{\sqrt{\Omega_{rc}}} \left(1 + \frac{aH'}{3H} \right). \quad (\text{B5})$$

The fully nonlinear modification in Hu-Sawicki $f(R)$ is given by ([Lombriser et al. 2014](#))

$$\mathcal{F}_{\text{fR}} = \min \left[O - O^2 + \frac{O^3}{3}, \frac{1}{3} \right], \quad (\text{B6})$$

¹¹ We note a typo appearing in Eq. C7 of [Bose et al. \(2020\)](#) where δ should have been $(\delta+1)$.

where

$$O = \frac{f_0 y_h a (3\Omega_{m,0} - 4)^2}{\Omega_{m,0} (R_i/a_i)^2} \times [\tilde{G}(y_{\text{env}}) - \tilde{G}(y_h)], \quad (\text{B7})$$

and

$$\tilde{G}(y) = \left[\frac{\Omega_{m,0}}{(ya)^3} + 4 - 4\Omega_{m,0} \right]^{-2}, \quad (\text{B8})$$

where y_h is the quantity solved for using $f(R)$ halos whereas y_{env} is that solved for in the environment, which is approximated by performing the same calculation but with $f_0 = 0$.

B2 nPPF forms

We also reproduce the nPPF expressions for both of these theories from [Lombriser \(2016\)](#). In DGP we have the following values for the p_i parameters in [Equation 39](#)

$$\begin{aligned} p_1 &= 2, & p_2 &= 1, & p_3 &= \frac{3}{2}, \\ p_4(a) &= 2 \left(\frac{\Omega_{m,0}}{4\Omega_{rc}} \frac{1}{9\beta(a)^2} \right)^{1/3}, & p_5 &= -1, & p_6 &= 0, \\ p_7 &= 0, \end{aligned} \quad (\text{B9})$$

which reproduce [Equation B1](#) exactly. Note if using [Equation 37](#) we simply set $p_2 = \frac{1}{3\beta(a)}$.

On the other hand, the Hu-Sawicki $f(R)$ parameterisation is not exact but is closely matched by the following parameters in the screening regime ([Lombriser 2016](#)) for a given choice of p_1 (using [Equation 39](#))

$$\begin{aligned} p_2 &= 1, & p_3 &= 7, \\ p_4 &= 2\Omega_{m,0}^{1/3} \left[(\Omega_{m,0} + 4(1 - \Omega_{m,0})^{-2} \frac{p_1}{3|f_{\text{R0}}|}) \right]^{1/p_3}, \\ p_5 &= -1, & p_6 &= \frac{2}{3p_3}, & p_7 &= -\frac{6}{7}, \end{aligned} \quad (\text{B10})$$

where we used $\alpha = 1/(n+1) = 0.5$ ([Lombriser et al. 2014](#)) in Equation 5.6 of [Lombriser \(2016\)](#). Again, if using [Equation 37](#) we set $p_2 = \frac{1}{3}$.

B3 Comparisons

Here we provide some comparisons of the approximate expressions for \mathcal{F} given by the nPPF model ([Equation 39](#)) and the Erf model ([Equation 41](#)) against the exact expressions in DGP ([Equation B1](#)) and $f(R)$ ([Equation B6](#)). Since the nPPF form is exact for DGP, we only compare it in the $f(R)$ case. Unless otherwise stated, the fits are performed as described in [section 5](#) and shown in [Table 3](#).

B3.1 DGP

In [Figure B1](#) we show the nonlinear modification to the Poisson equation, $1 + \mathcal{F}$, in DGP for $\Omega_{rc} = 0.25$ and $\Omega_{rc} = 0.01$ as a function of top-hat radius parameter y_h . We plot the exact solution given by [Equation B1](#) given as solid curves to the best fit Erf model given as dashed curves. We see an additional redshift dependence of the screening scale becoming important for high z . As modifications to GR are expected to be small at high redshift, this deviation may not be so important, which is supported by [Figure 4](#). We have performed a fit of this redshift dependence and find it behaves very well as a power law, with an $O(0.1)$ exponent (specifically ≤ 0.15), which

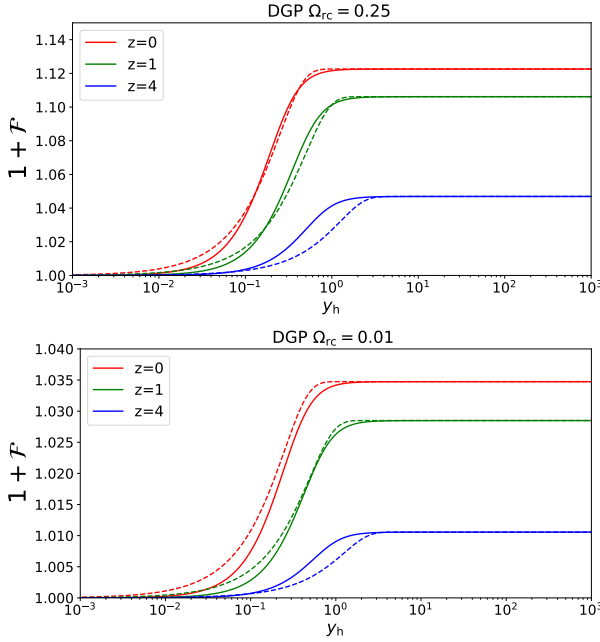


Figure B1. The modification to the Poisson equation $1 + \mathcal{F}$ (see Equation 13) in DGP gravity for $\Omega_{rc} = 0.25$ (left) and $\Omega_{rc} = 0.01$ (right). We plot the modifications as a function of normalised halo top-hat radius parameter for three different redshifts, $z = 0$ (red), $z = 1$ (green) and $z = 4$ (blue). The solid curves are the exact solution while the dashed curves are made using a single parameter fit to the exact \mathcal{R} using Equation 41 (see Table 3).

is first of all small and second of all degenerate with q_2 and q_3 , meaning the model likely has sufficient freedom to very well capture a DGP type of modification to gravity without biasing cosmological or gravitational constraints.

B3.2 Hu-Sawicki $f(R)$

Here we check that the nPPF and Erf models can qualitatively reproduce the exact form of \mathcal{F} (Equation B6) across all scales, masses and environments for Hu-Sawicki $f(R)$ gravity.

Before showing the results, we make a note on the best fitting parameters for the Erf model. We find that the fits in Table 3, performed by fitting the exact prediction for the reaction \mathcal{R} , do not give a very good agreement when comparing to the exact form of \mathcal{F} . In particular, we find that the mass dependence parameter, q_2 , seems to be underestimated when fitting \mathcal{R} . This parameter dictates the left hand slope in the contour plots in this section. Such a discrepancy may be due to a number of factors including a missing redshift dependency, the details of the fit, degeneracies with q_3 and failings of the power law description. We find a better by-eye fit for \mathcal{F}_{Erf} across redshifts $z = 0, 1, 4$ and all values of $|f_{R0}|$ is $q_2 = 0.85$. All other parameters are as in Table 3 unless otherwise stated.

In Figure B2 we show $1 + \mathcal{F}$ for the exact (top panels), the Erf (middle panels) and the nPPF (lower panels) cases with $|f_{R0}| = 10^{-5}$, characterising a moderate modification to Λ CDM. We do not show the $|f_{R0}| = 10^{-6}, 10^{-7}$ cases which are qualitatively similar.

To check the effects of Yukawa suppression, we set $y_{\text{env}} = 1$, which is the maximum value considered in the spherical collapse computation. We then plot \mathcal{F} as a function of dimensionless top-hat radius parameter y_h and halo mass, which shows the screening regime and the onset of Yukawa suppression. For large masses and redshifts, screening occurs at larger physical scales while Yukawa suppression

occurs at smaller scales. In all cases, the Yukawa suppression is only mildly relevant for $y_h \rightarrow y_{\text{env}}$ and very large masses. The nPPF best fit value of p_8 gives a wrong Yukawa suppression scale, which is likely due to its global fit over all values of y_{env} . Similarly, the Erf best fit screening scale, q_1 , is also underestimated, likely for the same reasons.

Further, the nPPF shows a good match for the redshift dependence of the screening scale, while the Erf fit does significantly worse. We recall the nPPF uses a theoretically matched power law for this dependence (see Equation 36 and Equation B10), while this dependence is fixed for the Erf case.

In Figure B3 we show $1 + \mathcal{F}$ for $|f_{R0}| = 10^{-5}$, with $y_{\text{env}} = 0.3$, again for all cases. We find a good qualitative agreement between the nPPF and exact solutions. On the other hand, the comparisons again show there is an inaccurate redshift dependency in the screening scale of the Erf model, set by q_1 . This was also seen in the DGP case. Despite this, the flexibility of the model still allows us to produce very accurate results at the power spectrum level (see Figure 5) and so we do not feel introducing new freedom is warranted. We leave this issue to be further investigated in future work.

B4 A note on notation

We would like to briefly discuss the inconsistency in the notation of previous related publications. The physical top-hat radius is denoted by R_{TH} in Cataneo et al. (2020); Bose et al. (2020), r in Carrilho et al. (2022), R in Schmidt (2010) and ξ in Lombriser et al. (2014). From the definition of the physical top-hat radius and the conservation of mass $M = 4\pi\bar{\rho}_m(\delta + 1)R_{\text{TH}}^3/3$ the expression for the nonlinear overdensity is correctly given in Equation B3. Note the corresponding typos in the definition of the nonlinear over-density of Cataneo et al. (2020); Bose et al. (2020); Carrilho et al. (2022) in Equations. 34, B3 and 28 respectively. The connection between the physical top-hat radius and the initial comoving radius R_{th} ¹² of the over-density is linear $R_{\text{TH}}(a_i) = R_i = a_i R_{\text{th}}$ initially but then due to the nonlinear evolution of the over-density it becomes $R_{\text{TH}}(a) = yaR_{\text{th}}$. This nonlinear evolution is encoded in the nonlinear scale factor ya with y given in Equation B4. Note that the expression for \mathcal{F} in $f(R)$ gravity in Equation A2 of Cataneo et al. (2020) and Equation. C15 of Bose et al. (2020) is taken from Lombriser et al. (2014) and includes R_{TH} which should be replaced by $R_{\text{th}} = R_i/a_i$. While \mathcal{F} in nDGP model from Schmidt (2010) is correctly given in these ReACT papers.

This paper has been typeset from a TeX/LaTeX file prepared by the author.

¹² Denoted R_{th} in the ReACT code.

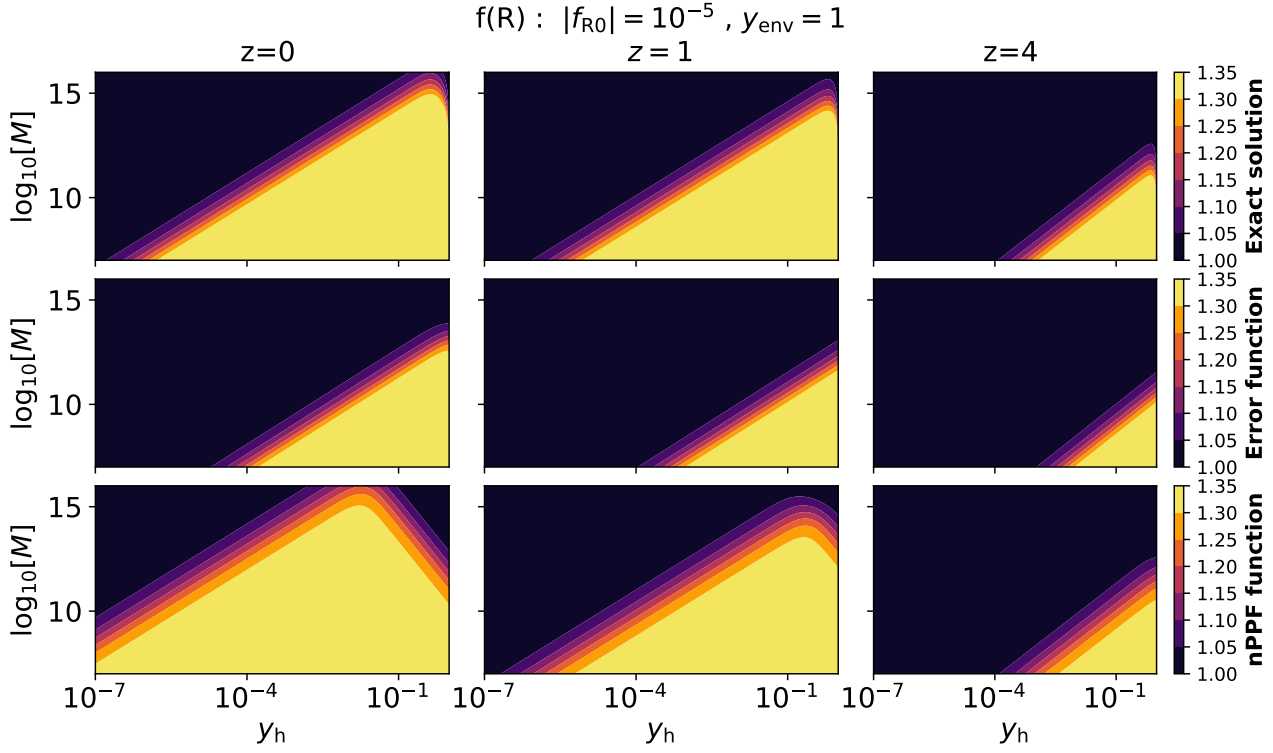


Figure B2. The modification to the Poisson equation $1 + \mathcal{F}$ (see Equation 13) in Hu-Sawicki $f(R)$ as a function of $\log_{10}(M)$ and top-hat radius parameter y_h . We set $|f_{R0}| = 10^{-5}$ and $y_{\text{env}} = 1$. The **top** panels show the exact solution, the **middle** panels show the phenomenological solution based on the error function and the **bottom** panels show the nPPF function. The **left** most column shows the functions for $z = 0$, the **middle** for $z = 1$ and the **right** most column for $z = 4$.

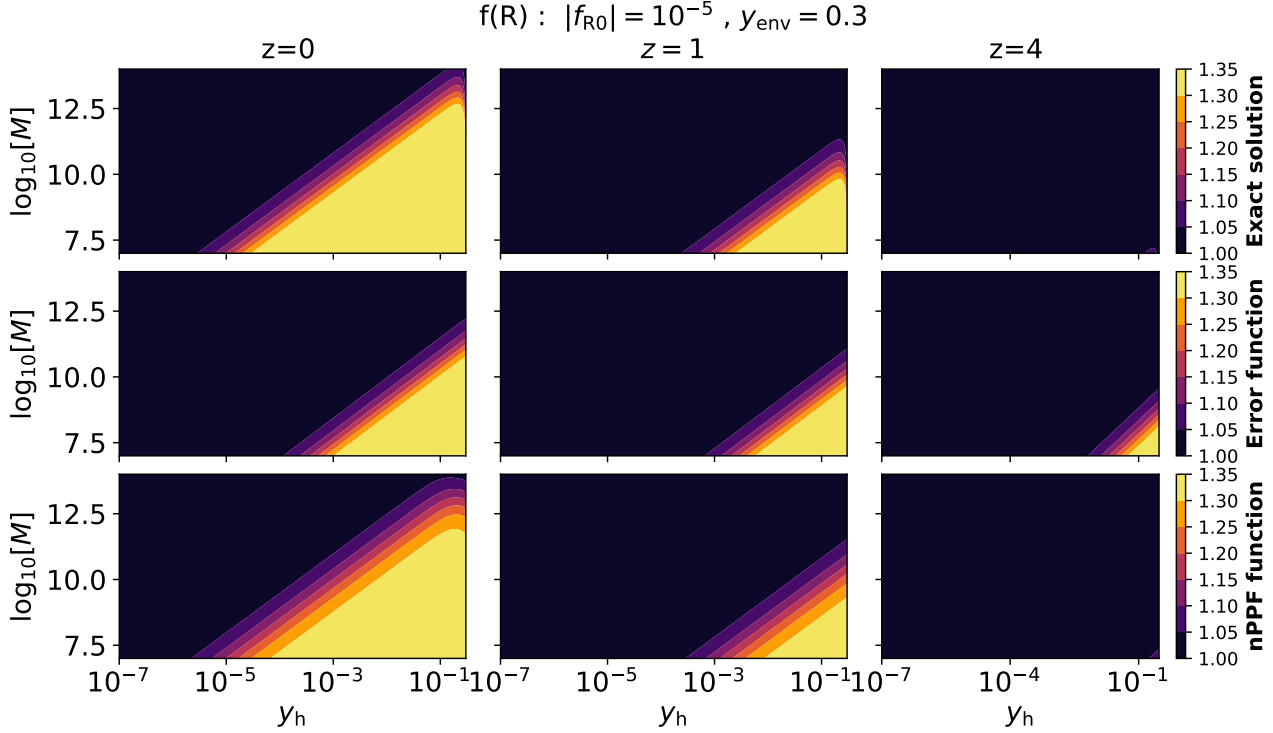


Figure B3. Same as Figure B2 but with $y_{\text{env}} = 0.3$.